Defense Nuclear Agency
Alexandria, VA 22310-3398

DNA-TR-92-12

Effects of Processing on MOS Radiation Hardening

Dr. Ralph J. Jaccodine
Dr. Donald R. Young
Lehigh University
Office of Research and Sponsored Programs
526 Brodhead Avenue
Bethlehem, PA 18015

September 1992

Technical Report

CONTRACT No. DNA 001-88-C-0122

Destroy this report when it is no longer needed. Do not return to sender.

PLEASE NOTIFY THE DEFENSE NUCLEAR AGENCY, ATTN: CSTI, 6801 TELEGRAPH ROAD, ALEXANDRIA, VA 22310-3398, IF YOUR ADDRESS IS INCORRECT, IF YOU WISH IT DELETED FROM THE DISTRIBUTION LIST, OR IF THE ADDRESSEE IS NO LONGER EMPLOYED BY YOUR ORGANIZATION.

REPORT DOCUMENTATION PAGE

Form Approved
OMB No. 0704-0188

1. AGENCY USE ONLY *(Leave blank)*	2. REPORT DATE	3. REPORT TYPE AND DATES COVERED
	920901	Technical 880827 - 920817

4. TITLE AND SUBTITLE

Effects of Processing on MOS Radiation Hardening

5. FUNDING NUMBERS

C - DNA 001-88-C-0122
PE - 62715H
PR - RV
TA - RA
WU - DH880122

6. AUTHOR(S)

Dr. Ralph J. Jaccodine and Dr. Donald R. Young

7. PERFORMING ORGANIZATION NAME(S) AND ADDRESS(ES)

Lehigh University
Office of Research and Sponsored Programs
526 Brodhead Avenue
Bethlehem, PA 18015

8. PERFORMING ORGANIZATION REPORT NUMBER

9. SPONSORING/MONITORING AGENCY NAME(S) AND ADDRESS(ES)

Defense Nuclear Agency
6801 Telegraph Road
Alexandria, VA 22310-3398
RAEE/Cohn

10. SPONSORING/MONITORING AGENCY REPORT NUMBER

DNA-TR-92-12

11. SUPPLEMENTARY NOTES

This work was sponsored by the Defense Nuclear Agency under RDT&E RMC Code B4662D RV RA 00226 RAEE 3400A 25904D.

12a. DISTRIBUTION/AVAILABILITY STATEMENT

Approved for public release; distribution is unlimited.

12b. DISTRIBUTION CODE

13. ABSTRACT *(Maximum 200 words)*

This study substantiated the beneficial effects of using fluorine as an additive during the oxidation of silicon for application to Insulated Gate-Field Effect transistor technology. The modern trend towards smaller devices makes it imperative to reduce the time and/or temperature required for the oxidation process. The dramatic increase in oxidation rates resulting from very small fluorine additions suggests the desirability of using fluorine.

The results of this study have clearly shown a significant reduction in the strain at the $Si-SiO_2$ interface, and in addition, a reduction in the oxidation enhanced stacking faults in the silicon. Electrical characterization confirmed the conclusion that the rise of fluorine is beneficial. The results are discussed.

In the course of this work, a relatively new technique was developed to use Q-V measurements to evaluate the interface and results of these measurements are included.

In summary, we are excited about the significant technological improvements that result from the use of fluorine during the oxidation process.

14. SUBJECT TERMS	15. NUMBER OF PAGES
Oxidation Fluorine Interface Measurements Point Defects	42
	16. PRICE CODE

17. SECURITY CLASSIFICATION OF REPORT	18. SECURITY CLASSIFICATION OF THIS PAGE	19. SECURITY CLASSIFICATION OF ABSTRACT	20. LIMITATION OF ABSTRACT
UNCLASSIFIED	UNCLASSIFIED	UNCLASSIFIED	SAR

CLASSIFIED BY:

N/A since Unclassified.

DECLASSIFY ON:

N/A since Unclassified.

SUMMARY

The objective for this study was aimed at the kinetics of growth of oxides using low concentration additions of Fluorine to the oxidant stream, the study of related oxidation phenomena such as strain and oxidation induced defects (stacking faults), and, importantly, the significance of fluorine, either grown in or implanted on, MOS properties and hot carrier trapping.

The experimental growth and measurements work carried out under this project has shown that this is a technologically successful, easily implemented process which has a major influence on interfacial strain and hot carrier trapping. During the course of these investigations, a new method of measuring interfaces was implemented which allows one to measure accurately and conveniently interface distribution without the use of C-V measurement.

The report will be organized along the following sections:

1) Oxidation kinetics with fluorine additions (NF_3 and dichlorofluorethane)

2) Influence of this process on stacking faults and strain characterization techniques

3) MOS characterization techniques and hot carrier trapping

Each of these tools was successfully carried out and objective met. Additionally, a great deal of insight and important information was uncovered during these studies. The investigators believe that this process is superior to present state-of-the-art practice.

In addition to the reduced (by two orders of magnitude) impurity inclusion for Fluorine sources vs. Chlorine sources, many of the other beneficial effects on point defects, traps, MOS quality, etc., are included in this study and make the above statement valid.

PREFACE

Permission has been granted by The Electrochemical Society, Inc. and the American Institute of Physics to use copyrighted information.

TABLE OF CONTENTS

FIGURES

SECTION 1

OXIDATION KINETICS

The first phase of our studies was to adapt "standard equipment" used in industry, i.e. horizontal thermal oxidation furnace to be used in the new process. The practical implementation of this process was to use standard high temperature (Mini Brute) furnaces modified with an appropriate gas handling and temperature controlled "bubbler" system capable of mixing the proper flows of impurity to oxidant gases. With this system, we established the experimental source, gas delivery system, apparatus and conditions of the study. The work established the growth characteristics of the SiO_2, as well as some of the influence of the amount of fluorine additions on the various growth parameters.

The early phases of this work were established in an M.S. Thesis by C. Wolowodiuk (Wolowodiuk, 1985) and later in a Ph.D. Thesis by U.S. Kim (Kim, 1990). Some of the most recent work has been summarized by Kim, Wolowodiuk, Jaccodine, et al. (Jaccodine, et al., 1990).

We have established first, that small amounts of a fluorine source (NF_3 or $C_2H_3Cl_2F$ in the region of .0x/100% - hundredths of a percent) greatly enhances the oxidation rate.

As can be seen in Figure 1 (Jaccodine, et al., 1990), there is a large enhancement of the dry oxide thickness with fluorine added compared to the other state-of-the-art sources, other industrial processes, even over that for a ten percent volume addition of HCl with as low an addition of 400 ppm. (by volume) of the Fluorine compound. In this same reference (Jaccodine, et al., 1990) is also summarized the effective B and B/A parameters for the Deal-Grove linear-parabolic model as well as the constant for the power of time model (Deal, Grove, 1965; Nicollian, Reisman, et al., 1987). These parameters define the relevant growth laws for this process.

One of the key findings of this earlier work, which was anticipated but was even more dramatically demonstrated, was the need for good control over the active Fluorine concentration. "Too much of a good thing" was found to be deleterious. This is a clear indication of the competition between oxide enhanced growth and the tendency for Fluorine species to act as an etchant of the growing oxide.

For the analyses of the growth kinetics previously mentioned, it was shown that Fluorine plays a key role in the structure of the oxide formed, namely the oxide structure was opened sufficiently for the parabolic rate constant (related to oxidant diffusion) to show a marked enhancement. The interface kinetics were also modified indicating that Fluorine acts almost catalytically with a resultant increase in the linear growth rate regime. Another measure of these effects was seen by the effect that F additions have on the dielectric properties and optical index.

The work in this part of the research was also aimed at specific kinetic information on the new processes. We have explored this issue and have

discussed the kinetic data in terms of both the more traditional Deal-Grove (linear-parabolic) model (Deal, Grove, 1965) and also using the power of time model favored by E. Nicollian and A. Reisman (Nicollian, Reisman, et al., 1987).

This information is found in tabulation of temperature and fluorine impurity and concentration in Table II and Table III as noted in (Jaccodine, et al., 1990).

In addition, the resultant inclusion of Fluorine in the SiO_2 was studied as a function of the two "generic" sources used in the kinetic study by SIMS. It was a finding of this work that the shape of the (F) profile depended on when it was introduced into the growth process, as well as the type of the source impurity used. Specifically, these profiles were highly dependent on the "dryness" of the oxidation. It was postulated (to explain this date) that, with hydroxides present, F will move by a replacement reaction similar to that which occurs for Cl. In contrast with our NF_3 source and dry oxidation, the F profiles are generally quite flat and "saturaced" through the oxide.

SECTION 2

INFLUENCE OF PROCESS ON DEFECTS AND "OTHER EFFECTS"

This area covers important "other effects" that are a consequence of or bear on the technology of oxidation. Oxides grown by the new process were examined for any anomalous breakdown or ionic migration behavior. These oxides were shown to be as good as those of the best present practice, and every indication is that F acts as an efficient materials getter for impurities.

More pertinent, because it represents new findings, is the role F plays in suppressing oxidation induced stacking faults. It was conjectured in our proposed work that fluorine may be able to suppress stacking fault nucleation and growth; in fact, it was extremely effective for this purpose. We investigated the behavior of oxidation induced stacking faults (OSF's) during fluorine-oxidation in temperature range 850° - 1100 ° C. It was observed that pregrown OSF's shrink very rapidly and that no OSF's are generated even when damage is purposely done to the wafers prior to oxidation. This work (Jaccodine, Kim, 1986) also showed that the activation energy for shrinkage is much lower than for other comparable processes. This is shown in Figure 2. The more complete findings of this work are published in Lehigh Ph.D. Thesis by U.S. Kim (Kim, 1990).

One of the unexpected results of this work is that the new F oxidation process completely reverses the normal point defects balance at the growth interface such that vacancies are induced over the equilibrium concentration $C_v > C_v$ eq. and that these vacancies (instead of interstitial silicon) are injected back into the substrate. The important implication of this is that oxidation enhanced/retarded diffusion effects are reversed over those normally expected (Kim, 1990).

As a part of our general investigation, we anticipated that a few other fluorine containing additives may be also readily useful sources. We also expected that a great deal of trial and error substitution of additive gases would be required. It was quite clear that the original source (Dichlorofluorethane - $C_2H_3Cl_2F$) we selected and used had very convenient handling and vapor pressure properties for easy replacement into a state-of-the-art oxidation facility. This is where the work started. It became also obvious by considering the SIMS profiles of included F in the oxides that the presence of hydrogen in this source resulted in an effective "wet" oxide. This was also seen in growth rate vs. temperature results. Our next step was to investigate a source with neither H or the Cl. This source NF_3 turned out to be the simplest and most flexible and useful of the ones investigated. All the work by Wolowodiuk, Kim, McCluskey and Huang (theses and publications) were carried out using one or other of these two sources.

In order to come to grips with the potential multitude of available Freon-like sources (Freon 11, 12, 22, etc.), we not only explored the literature for current use but importantly we used the SOLGAS program (Eriksson, 1971) to calibrate the partial pressure of possible oxidizing species under the actual high temperature oxidation conditions in the furnace.

These calculations could be accomplished for all the reasonable source families that were considered provided sufficient thermodynamic information was available. In that way families of like compounds could be compared to give insight into what species were responsible for enhancing rates, etc. For example, the $C_2H_3Cl_2F$ source that gave strong indications as to the important actual species partial pressures that were different and thus effective for understanding the process.

This simulation and calculation techniques were also employed to explore (theoretically) the role of small additions of H_2 (and, of course, H_2O) to the ambient. This approach also allowed us to recognize the advantages of the use of the NF_3 source. This can also be seen in Figure 3 (Kim, 1990) which is a plot of partial pressure in N-F-O-H system vs. a function of temperature.

By means of these calculations and simulations, many experimental conditions and source compositions could be compared without the need for the large expenditure of effort, materials and cost entailed in one for one comparison experimental work.

Guided by these programs, we then took the most attractive resources and committed these to the experimental studies.

The analytic work involved the determination of the F concentration in depth in the oxide and its role on mechanical properties was included as part of all the experimental studies. Data from SIMS was obtained from many samples. A sample of the different resulting F concentration from both sources can be seen from the Figures 4 and 5 (Jaccodine, et al., 1990).

Figure 4 is illustrative of the "peaked" concentration when the presence of H_2 in the source allows H_2O-F replacement reaction to occur. Figure 5 shows an example of the "saturated" level concentration using the NF_3 source and very dry conditions. Further details of this work and particularly the work in which the Fluorine was included as pulses during oxidation processes are now part of the Lehigh Thesis of Dimitrios Kouvatsos (Kouvatsos, 1991).

Study of Interfacial Strain as a function of F concentration was carried out and reported in Lehigh thesis of D. Kouvatsos (Kouvatsos, 1991) in Chapter 3. As shown in this work, oxide stress as measured optically is markedly reduced when the concentration of additive NF_3 exceeds 100 ppm in the oxides grown from 800° - 100° C (Figure 6). Additional work was done to profile the stress throughout the thickness of the oxide both dry and with NF_3 addition. It was shown in this study (Figure 7) that again the total stress was relieved with NF_3 addition but also a variation of stress as a function of depth for oxides grown at 1000° C. This effect is less dramatic than 900° C and more dramatic than 1000° C for 1100° C.

SECTION 3

MOS CHARACTERIZATION TECHNIQUES AND HOT CARRIER TRAPPING

The electrical characteristics of Si-SiO_2 interface:

The beneficial effects of using fluorine in the oxidation process have been described elsewhere in this report. The objective for this part of the work has been to investigate the effect of fluorine on the electrical characteristics of SiO_2 and its interface with silicon. The equipment available for this investigation consists of the routine equipment normally used such as high frequency C-V measurements, quasi static measurements and high field injection current measurements.

In addition to this type of equipment we have an automatic avalanche injection apparatus that was originally designed by one of the authors (D. Young) while he was at IBM Yorktown Heights Research Laboratory and subsequently donated to Lehigh by IBM. The results of these studies, using this equipment, enable us to determine the cross section and density of the traps involved. The injected carriers can be either electrons or holes as desired. This apparatus makes it possible to pass a constant current through the sample using a silicon avalanche injection process. this current can be set as desired over a wide range. For the study of large cross section traps a large current is used. The injection process is periodically halted (for example, every 100 sec.) and the resultant trapped charge measured by automatic high frequency C-V measurements. The results are stored in a personal computer and can be subsequently analyzed to determine the trap characteristics.

Since this apparatus runs automatically, a large number of measurements (200-500, for example) can be made, and in some cases it has been possible to measure three different traps for one particular run. This large cross section traps are filled first and then the smaller cross section traps are filled subsequently. The means for analyzing the data has been described in numerous previous publications (Young, 1981) and will not be repeated here.

The trend in modern semiconductor technology to use thinner insulators (down to 100 Å, for example) has placed increasing emphasis on the properties of the interface as compared to bulk effects. To enable us to learn more about the interface we have designed a special apparatus to measure in a relatively direct way the interface potential as a function of voltage applied to the gate electrode. The technique for making this measurement that we have used is called the Q-V technique. By comparison of the results of this measurement of interface potential as a function of the applied gate voltage, we are able to determine the interface state distribution without the use of C-V measurements. This technique has many advantages that include the possibility of making the measurements over the entire band gap of silicon using only one sample, the interface potential measurements are independent of the interface state density. However, the results of the interface potential vs. the applied gate voltage do depend on the interface state densities and a comparison of our measured results with the ideal curves of interface potential vs. applied voltage enables us to determine the interface state

density. This compression is made without the use of capacity measurements or capacity calculations which is unique for our work. We have also used this apparatus to evaluate the effect of fluorine.

The results of measurements of trapped charge as a function of time resulting from the passage of electron current are frequently complicated by the competing mechanisms of negative charge build up in the bulk of the oxide and positive charge build up due to the generation of slow states at the interface. In addition, we also have observed the build up of fast states at the interface. We have been able to separate these effects by means of techniques developed in our laboratory. One significant means to do this is the use of an elevated temperature for the injection (120°C). This essentially eliminates the charge build up due to the slow states. There are two reasons for this: this temperature anneals out some of the these states as they are generated and, in addition, under conditions of our measurements the states tend to be discharged at these temperatures and hence do not contribute to the results. As a result, we are able to evaluate bulk charge trapping effects without this complication. During the course of this work we have also observed a significant decrease in the generation of fast interface states at 120°C (Figure 8).

Most of the results to be briefly described are based on the work of Dunxian Xie and are described in detail in his Ph.D. dissertation. This work has been published in the Journal of Applied Physics (Xie, Young, 1991). A copy of this paper is enclosed. The equipment for the Q-V measurements was designed by Ta-Cheng Lin and his work is described by a paper that has been accepted for publication in the Journal of Applied Physics. New means are used to determine the unknown constant in the Q-V measurement and, in addition, the technique for determining the interface state density distribution uses a comparison of the measured interface potential as a function of applied gate voltage with the calculated potential vs. gate voltage curve. Using this method we do not involve capacity measurements as is usually done.

SECTION 4

SUMMARY OF EXPERIMENTAL RESULTS

A brief summary of the results is given below. For a more complete discussion, see the paper included with this report.

Initially the fluorine was applied during the oxidation of the wafers. We were concerned about the purity of the gases we were using for this purpose and to be certain that our results were not due to impurities we shifted to the use of implantation as a source of fluorine. The use of implantation also made it easy to conduct comparison experiments since the fluorine can be implanted over part of the wafer and the remaining part of the wafer was used for comparison with the non-implanted case. There is always concern with the use of implantation that the results might be due to the implantation damage and not due to the chemical impurity. We have annealed all of our samples at 1000°C after the implantation to hopefully eliminate the radiation damage. To check on this we have implanted an inert species Ne^+ and the results are similar to the non-implanted case so we conclude that, for the purpose of our experiments, implantation damage is not playing a significant role (Figure 5 of the enclosed publication).

One of the complications of electron injection-trapping experiments is that the effective trapped charge does not build up monitonically but there is a turn around in the characteristics which is known to be due to the build up of positive charge at the interface due to the formation of slow donor states as a result of the passage of electron current (Dekeersmaecker, et al., 1979). Our results with fluorinated samples also show this effect as shown in Figure 2 of the publication enclosed. However, we also observe that for a particular implantation dose of $10^{14}/cm^2$ this effect disappears.

The increase in electron trapping rate as a result of fluorine is to be expected since it is generally observed that the addition of chemically active impurities increases the electron trapping rate of SiO_2. Many of the other modifications of SiO_2 that are being considered have the same effect such as the use of oxinitrides. It is interesting to note that for the case of fluorine, the cross section of the traps involved is in the range of 10^{-17}-$10^{19}/cm^2$. These relatively small cross sections are not of concern for device operation since they would not be filled under normal conditions of device operation. It would require a very long time to fill these traps with the injected current density present with operating devices. The traps of concern have much larger cross sections than these.

It has also been observed that there is a larger stretch out in the C-V curves for the fluorinated oxides as a result of electron injection suggesting the generation of fast interface states. To investigate the effect this has on our measurements, we have followed the suggestion originally made by Lai and Young and compared the flat band voltage shift measured at flat band with the shift measured at mid-gap. The suggestion was that the interface states would not be charged at mid-gap. The observed shift is much larger at mid-gap (Figure 6 of enclosed publication). It appears that the relatively smaller shift observed at flat band is due to the compensation of the bulk negative

charge due to trapped electrons by the positive interface charge due ot donor-like interface states. Measurements made at an elevated temperature (120° C) also show that these differences tend to disappear indicating that these states are being annealed out during the electron injection process.

As a result of the application of a fluence of injected electrons, the capacity in the depletion region decreases. This has been investigated extensively by C.T. Sah and his students (Pan, Sah, 1987). They have explained this effect as being due to the release of hydrogen by the electron trapping process which diffuses to the interface and into the silicon. In the silicon, the hydrogen forms complexes with the boron dopant impurity and renders it ineffective as a dopant. We have observed that implanted fluorine enhances this effect. This enhancement might be due to the increased hydrogen diffusion due to implanted fluorine. These results are shown in Figures 9 and 10 where the results for the unimplanted sample are compared with the implanted sample.

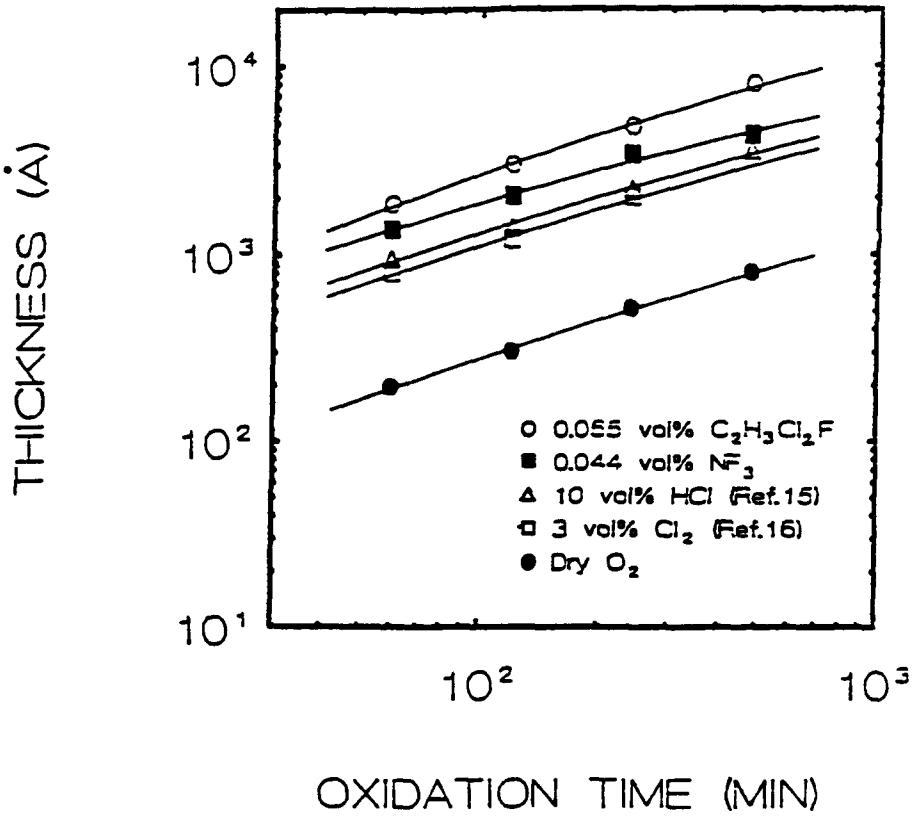

Figure 1. Oxide thickness vs. oxidation time for the oxidation of lightly doped silicon in various gas ambients at 1000°C. The points represent the experimental data. Solid line is the least squares fit with the power of time.

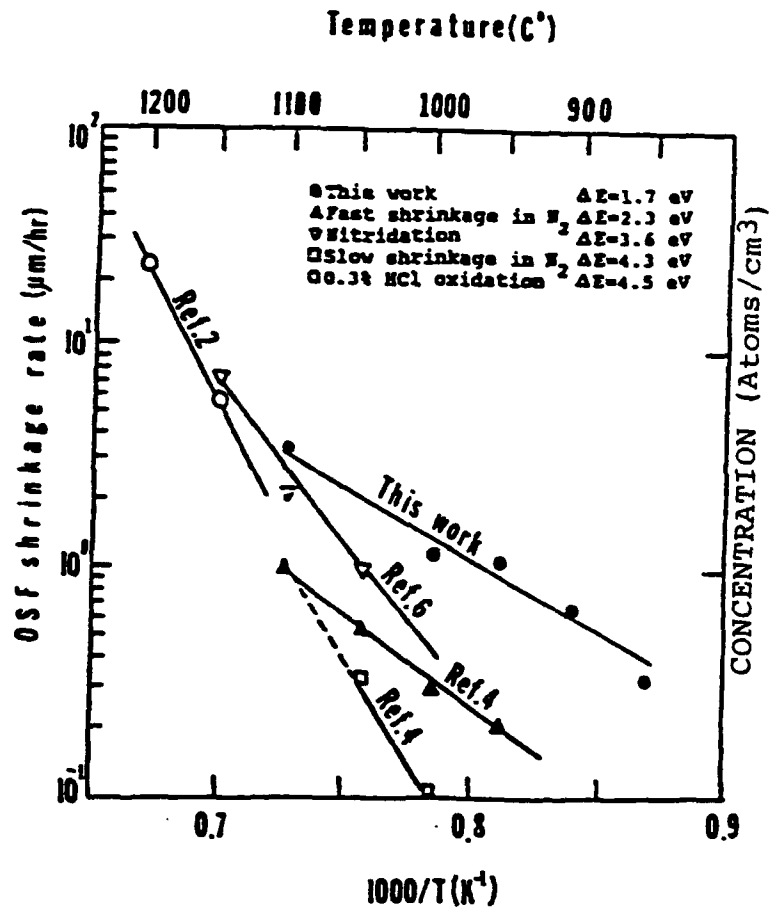

Figure 2. OSF shrinkage rates in various thermal heat treatments.

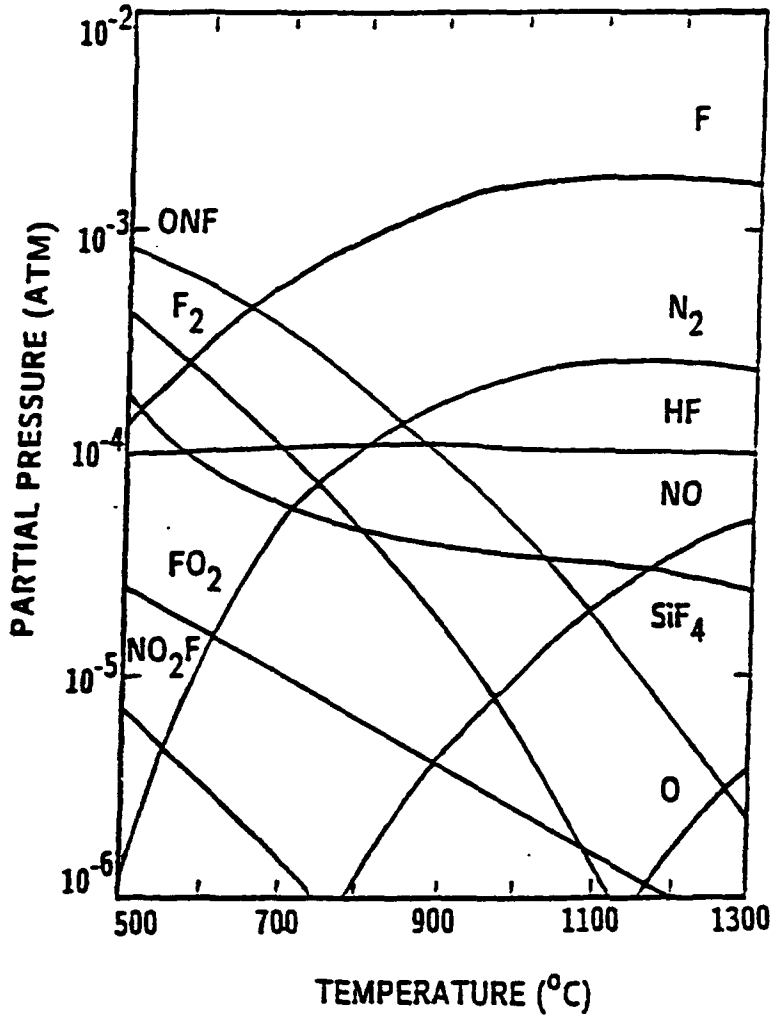

Figure 3. Equilibrium partial pressure in N-F-O-H system vs. temperature. (Total pressure = 1 atm, NF_3 = 0.044 vol% and H_2 = 0.005 vol%).

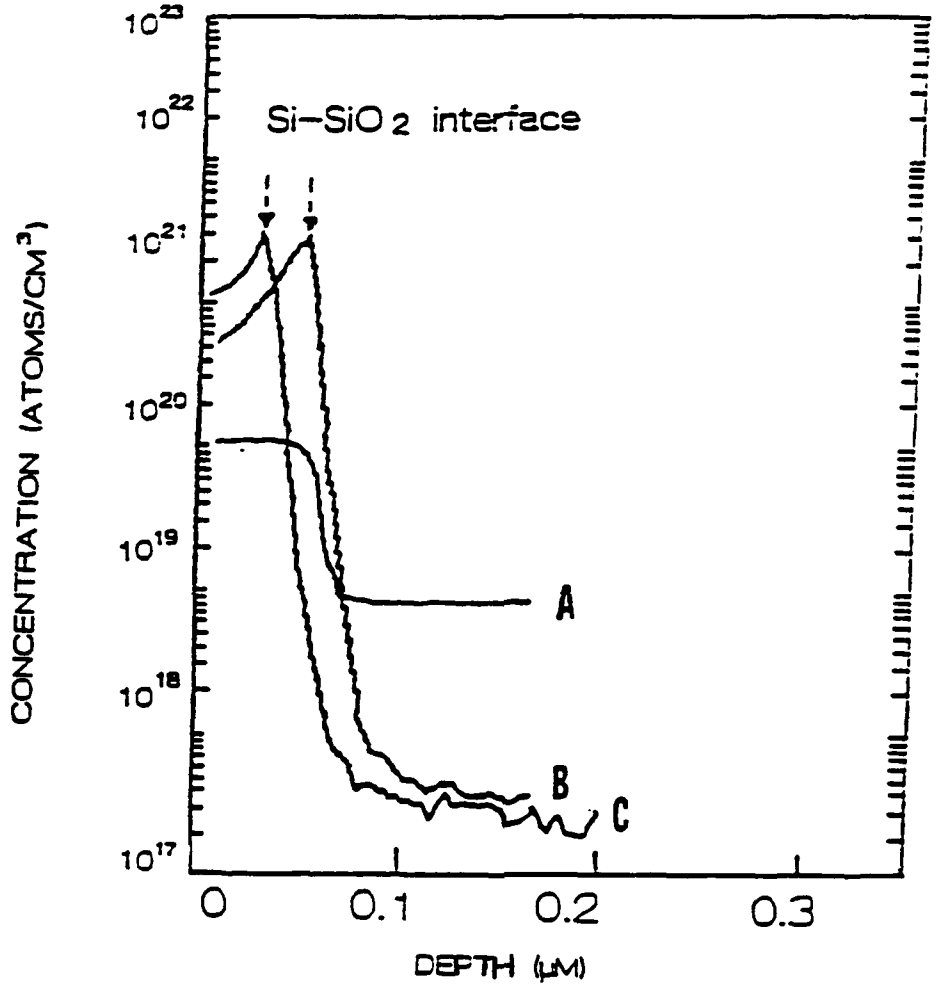

Figure 4. Fluorine and oxygen profiles of an oxide grown at 800°C with 0.011 v/o $C_2H_3Cl_2F$ in O_2. A, oxygen profile; B, 8h and C, 2h.

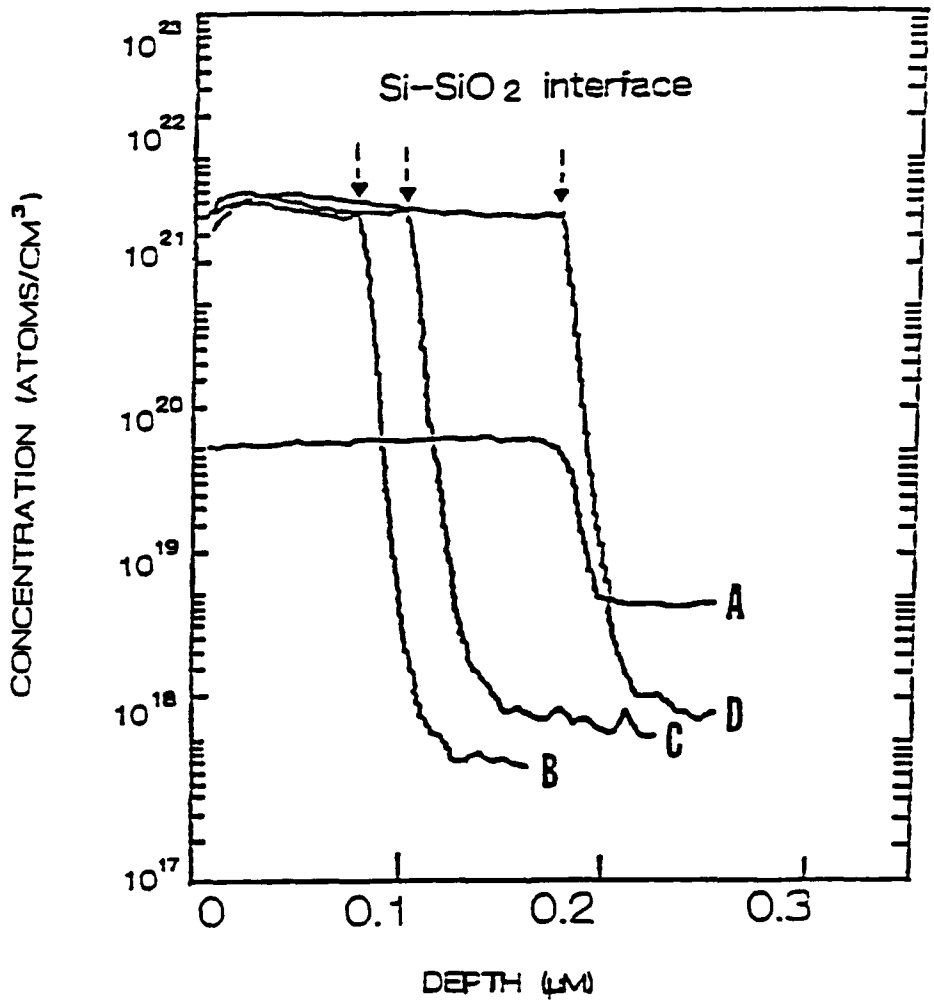

Figure 5. Fluorine and oxygen profiles of oxygen grown in different amounts of NF_3 addition at 900°C. A, oxygen profiles; B, 2h 0.011% NF_3; C, 2h 0.033% NF_3; D, 4h 0.022% NF_3.

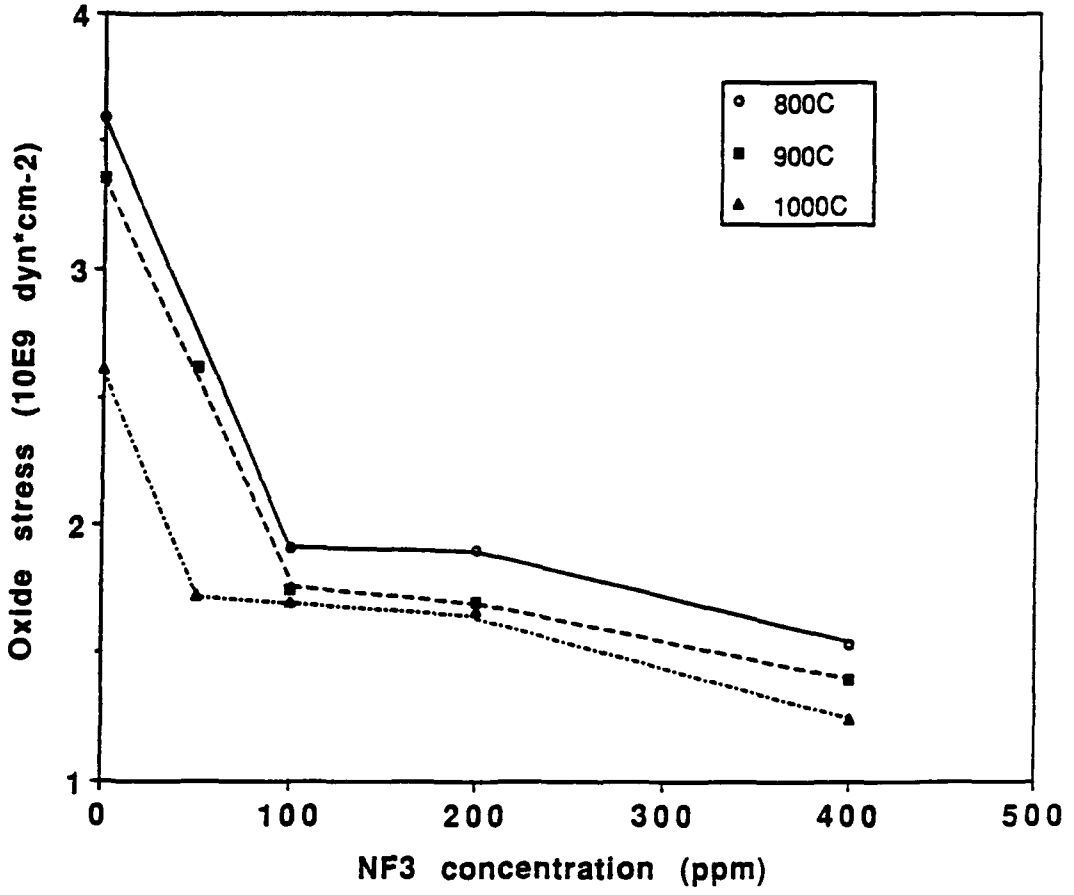

Figure 6. Oxide stress against NF_3 concentration with oxidation temperature as parameter.

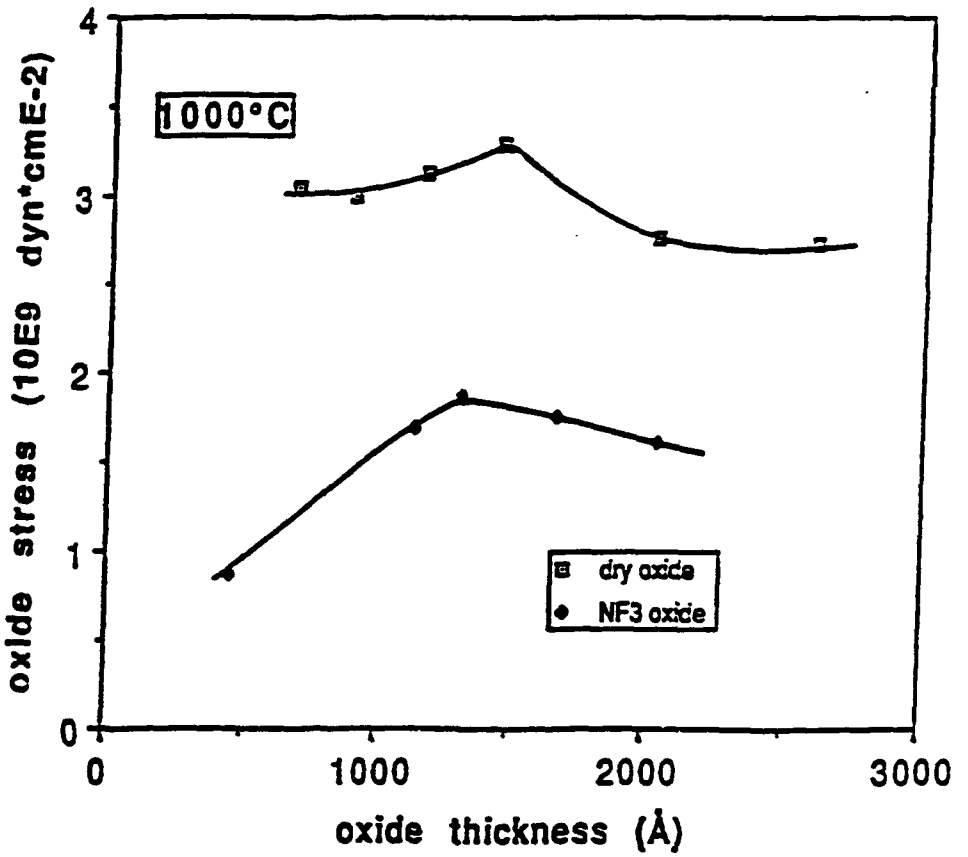

Figure 7. Oxide stress against thickness for dry and fluorinated oxides, oxidation at 1000°C.

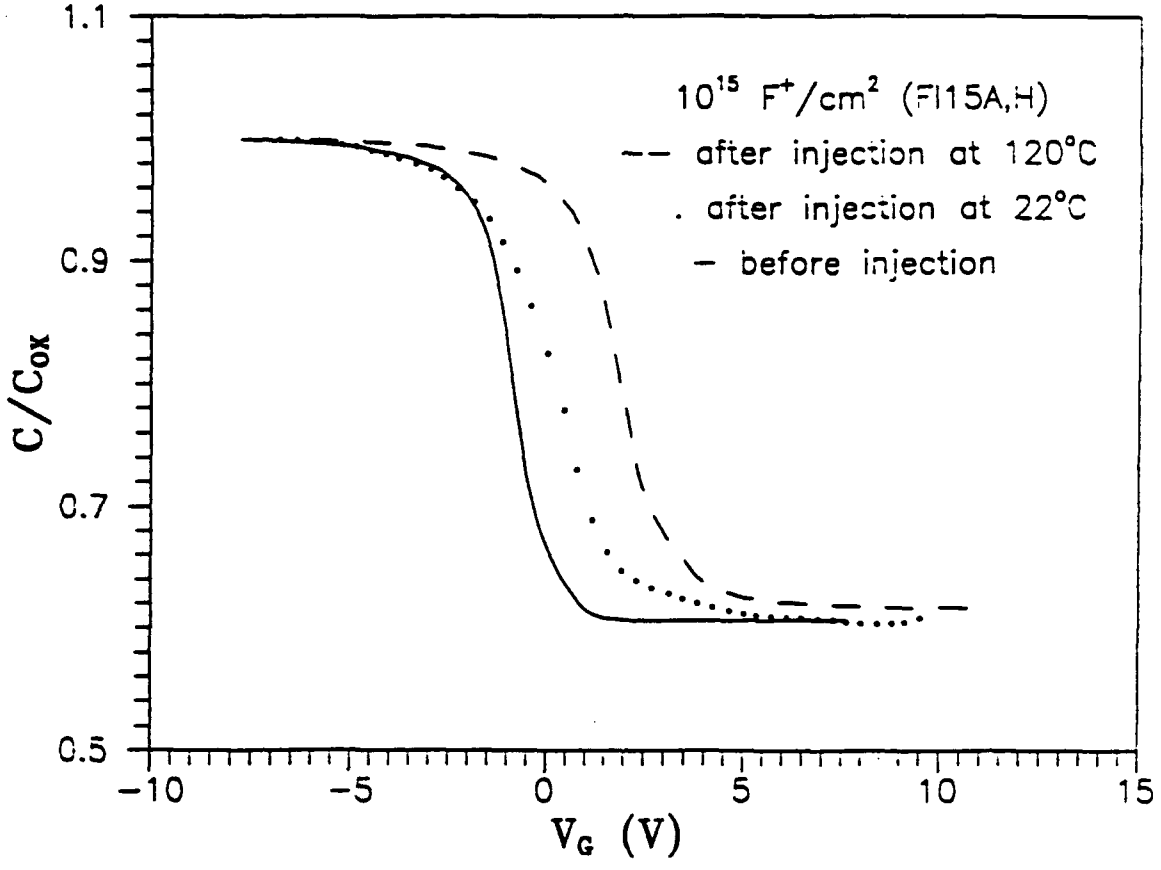

Figure 8. High frequency C-V curves before and after injection (dose: 10^{15} F^+/cm^2; d_{ox}=825Å; current density: $2x10^{-5}$ F^+/cm^2). The C-V curve after room temperature injection shows a stretch-out while the curve after high temperature injection shows a parallel shift.

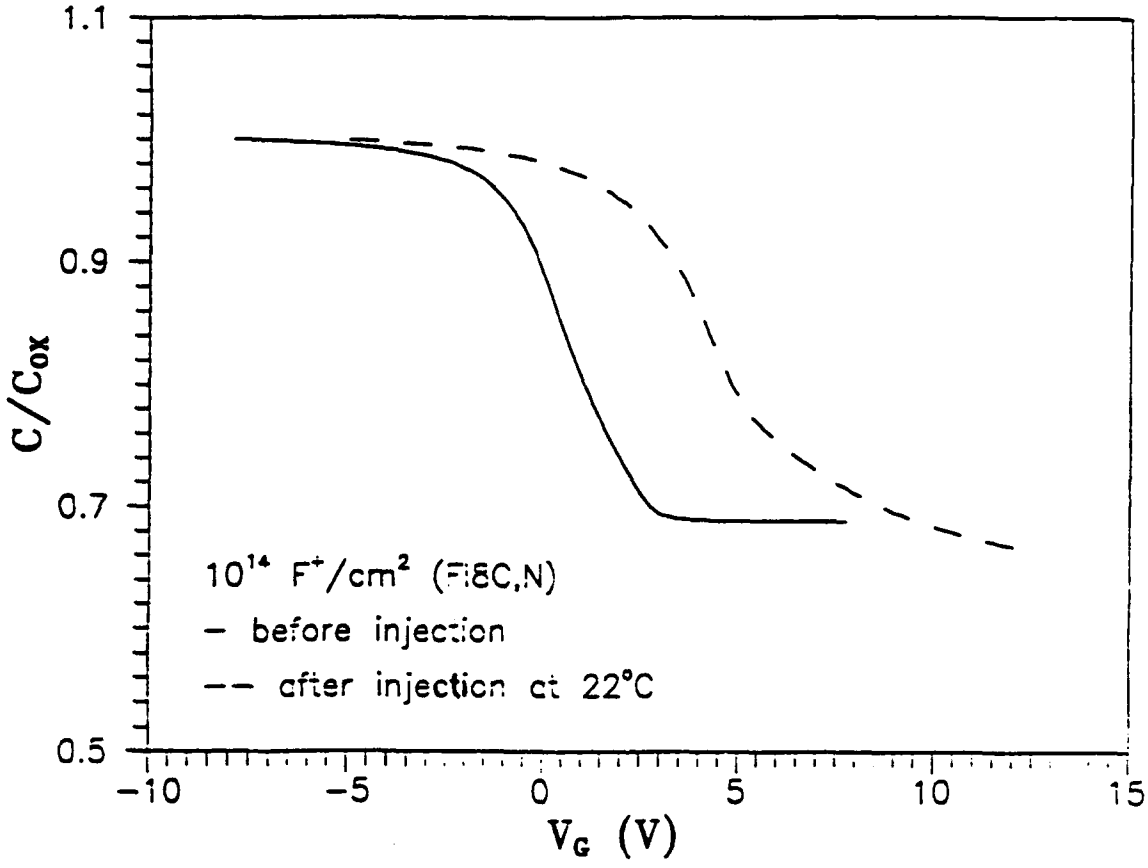

Figure 9. Decrease of minimum capacitance after room temperature injection (dose: 10^{15} F^+/cm^2; d_{ox}=600Å; current density: 2.2×10^{15} A/cm^2; injection fluence: 1.9 C/cm^2). A decrease of minimum capacitance results from a decrease of effective doping concentration in the silicon substrate.

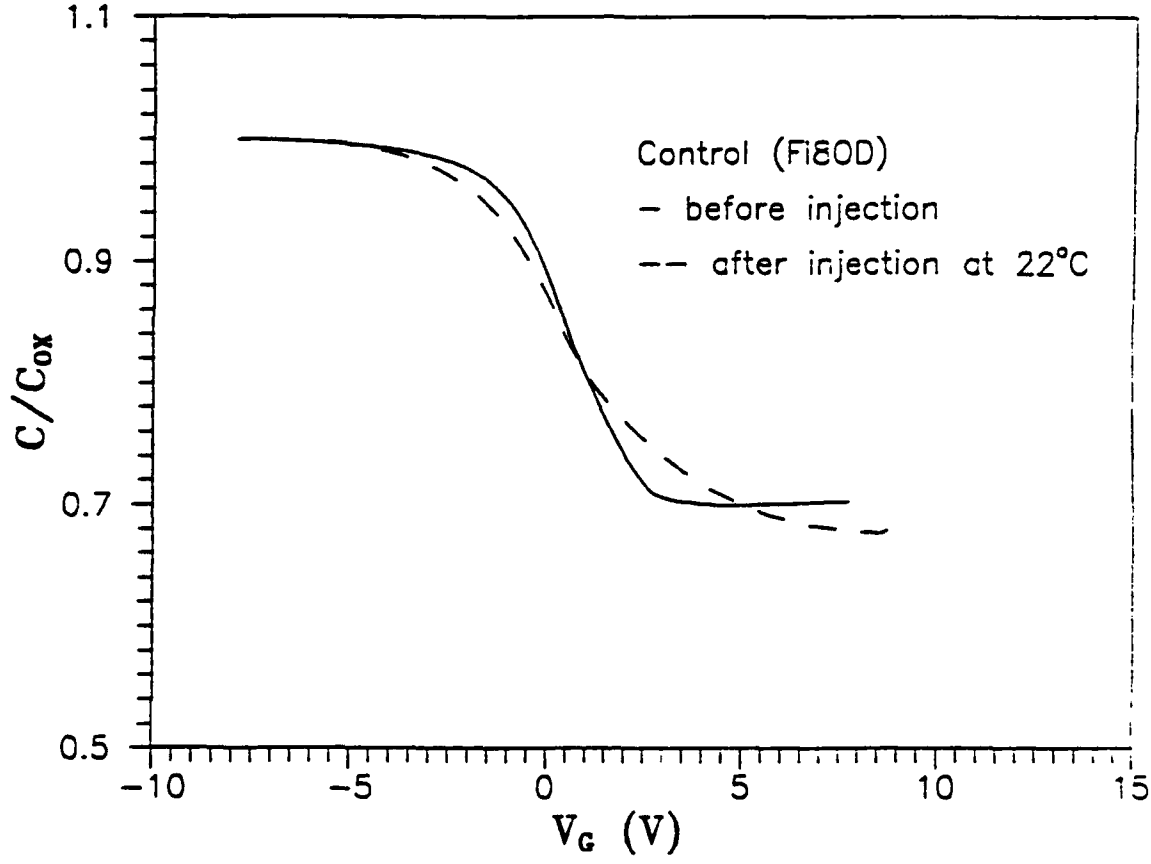

Figure 10. Decrease of minimum capacitance after room temperature injection (control oxide; d_{ox} = 600 Å; current density: 2.35×10^{-3} A/cm^2; injection fluence: 2.06 C/cm^2). A decrease of minimum capacitance results from a decrease of effective doping concentration in the silicon substrate.

SECTION 5

REFERENCES

Deal, B. and Grove, H., J. Appl. Phys. 36, 3770 (1965).

Dekeersmaecker, R.F., DiMaria, D.J., Irene, E.A., Massoud, H.Z., Young, D.R., J. Appl. Phys. 50, 6366 (1979).

Eriksson, G., Acta Chem. Scand., Vol. 26, pg. 2651 (1971).

Jaccodine, R. and Kim, U.S., Appl. Phys. Lett. 49 (18), pg. 1201, (1986).

Jaccodine, R.J., Kim, U.S., Wolowodiuk, C., et al., Electrochemical Society, Vol. 137, pgs. 2291-2294, July, (1990).

Kim, U.S., Ph.D. Thesis, Lehigh University, (1990).

Kouvatsos, D., Ph.D. Thesis, Lehigh University, (1991).

Nicollian, E., Reisman, A., et al., J. Electron. Material, Vol. 16, pg. 45, (1987).

Pan, S.Cheng-Seng and Sah, Chih-Tang, Appl. Phys. Lett. 51, 334 (1987).

Wolowodiuk, C., M.S. Thesis, Lehigh University, (1985).

Xie, D., Young, D.R., J. Appl. Phys. 70, 2755 (1991).

Young, D.R., J. Appl. Phys. 52, 4090 (1981).

APPENDIX A

The Effect of Fluorine Additions to the Oxidation of Silicon

U. S. Kim, C. H. Wolowodiuk,[1] and R. J. Jaccodine*

Sherman Fairchild Center for Solid State Studies, Lehigh University, Bethlehem, Pennsylvania 18015

F. Stevie and P. Kahora

AT&T Bell Laboratories, Allentown, Pennsylvania 18013

ABSTRACT

Experiments were carried out to study the effects of fluorine additions to a dry oxidation ambient. Two distinct classes of fluorine sources, liquid dichlorofluoroethane ($C_2H_3Cl_2F$), and gaseous nitrogen trifluoride (NF_3), were investigated. We experimentally found that small fluorine additions (up to 0.11% by volume) caused large enhancements in oxidation kinetics. The oxidation kinetics data were analyzed by both the power of time and linear-parabolic models as a function of fluorine addition, temperature, and the type of fluorine additive. Thermodynamic calculations for these classes of fluorine sources were extensively carried out to determine the active oxidizing species that cause the significant enhancement of the oxidation. According to these calculations, the enhancement of oxidation could be explained by the presence of hydrogen fluoride (HF) and atomic fluorine (F). Secondary ion mass spectrometry (SIMS) was performed to study the incorporation behavior of fluorine into the oxide layer. $C_2H_3Cl_2F$ oxides displayed peaks at the silicon-oxide interface, while NF_3 oxides exhibited flat fluorine profiles.

The addition of percent concentrations of a chlorine bearing compound to the silicon oxidation process has been widely practiced in silicon integrated circuit processing technology (1, 2). A new process has been reported (3-5) showing that small additions of fluorine in the parts per million range can result in a greatly enhanced oxidation rate as well as improved dielectric strength. Additional benefits of fluorine additions include the elimination of oxidation induced stacking faults (6), the retardation of boron diffusion (7), and, as reported by Ma and his coworkers (8), improved radiation resistance of oxide.

In this paper, experimental data showing the effect of fluorine additives on the growth kinetics of dry oxide as a function of the volume percent (v/o) addition of a fluorine source compound is presented. Two different classes of fluorine compounds were selected, namely, dichlorofluoroethane and gaseous nitrogen trifluoride. The alphatic liquid hydrocarbon, dichlorofluoroethane ($C_2H_3Cl_2F$), has an appropriate vapor pressure at room temperature for delivery by a gas bubbler system. Nitrogen fluoride (NF_3) is a gas that can be easily diluted and delivered directly into an oxidation gas system. The former source is easy to handle and combines both fluorine and chlorine species whereas the NF_3 has only fluorine and contains none of the additional carbon and hydrogen species as does the liquid source.

The SOLGAS program (9) was used to calculate the partial pressure of possible oxidizing species under oxidation conditions to ascertain which of the many possible sources would be suitable. This program was also used for assessing which specific species correlate with the enhanced oxidation rate. Fluorine profiles in the oxide and silicon were determined using secondary ion mass spectroscopy (SIMS). Oxidation kinetics data were used as guides to infer which physical processes are being influenced and enhanced, and thus lead to the marked enhancement in oxidation kinetics. Data were fit to the traditional linear-parabolic treatment (10) and also to the power of time model, the latter providing a better fit (11, 12).

Experimental

The silicon wafers used were chem-mechanically polished p-type, Czochralski-grown crystals of (100) orientation, with a resistivity of 2-10 Ω/cm. Oxides were grown by inserting wafers into the furnace tube in flowing N_2 and then switching over to the oxidant supply. The oxidizing gas flow for $O_2/C_2H_3Cl_2F$ oxidations was composed of 1 liter/min of oxygen (O_2) along with a much smaller flow of $C_2H_3Cl_2F$. The bubbler filled with the $C_2H_3Cl_2F$ was kept at room temperature, while oxygen was bubbled through at rates from 1 to 10 ml/min. This corresponded to fluorine additions from 0.011 to 0.11 v/o. NF_3 is a gaseous fluorine source, and its gas flow was monitored directly by microflowmeter before introduction into the oxidation furnace. Again, the oxidizing gas flow was controlled at 1 liter/min O_2 plus the addition of NF_3. The NF_3 additions were from 0.011 to 0.044 v/o. The oxidations were carried out in a conventional quartz furnace after a standard RCA cleaning for various times at 900° and 1000°C. Oxide thickness and refractive index were determined by a Rudolph Research Auto EL-II ellipsometer using a helium-neon laser. Physical integrity of the oxides was observed by optical and scanning electron microscopy (SEM).

The calculated concentrations of the various chemical species existing in the oxidation furnace were determined using the SOLGAS program, which computes the partial pressures of all the possible species in equilibrium in the system (9). JANAF thermodynamic data (entropy, enthalpy) (13) for all the species in the system and the number of moles of each element with stoichiometric coefficients were an input into the program, along with temperature. The total pressure, temperature, and initial input gas mixture were assumed to be constant throughout the process. To determine the effect of fluorine additions on an active species present at high temperature, two different systems containing fluorine were initially considered. For the $O_2/C_2H_3Cl_2F$ oxidation, as a model for the general class of hydrocarbons containing hydrogen, fluorine, and chlorine, the input data consisted of 0.11 v/o $C_2H_3Cl_2F$ in an O_2 ambient, for different temperatures. For O_2/NF_3 oxidation, as a model for the general class of some Freons not containing hydrogen and chlorine, the program was initially run at 0.11 v/o NF_3 as a function of temperature, and later rerun under the same conditions but with the addition (ppm) of hydrogen (H_2) to simulate the hydrocarbon impurities in the O_2 and the in-diffusion of moisture. The latter condition was thought to be the actual composition within the furnace.

Secondary ion mass spectrometry (SIMS) was performed to determine the fluorine concentration *vs.* depth profile in the oxides. The oxide films were rastered using Cs^+ ions across a 500 × 500 μm square at a rate of 12-16 Å/min. The fluorine profile was determined by monitoring $^{46}SiF^+$, which is equivalent to directly monitoring $^{19}F^+$. These rates have been verified by comparing the original oxide thickness measurement with the position of the run $^{46}SiF^+$ and $^{16}O^+$ profiles. Quantitative SIMS analysis requires standards of similar composition to the unknown. Since no fluorinated thermal silicon dioxide standards exist, we used a F-implanted standard typically with <<1% F. In particular, it was observed that the film density decreases with fluorine incorporation. This matrix effect complicates the analyses and thus the fluorine concen-

* Electrochemical Society Active Member.
[1] Present address: Shipley Corporation, Newton, Massachusetts 02162.

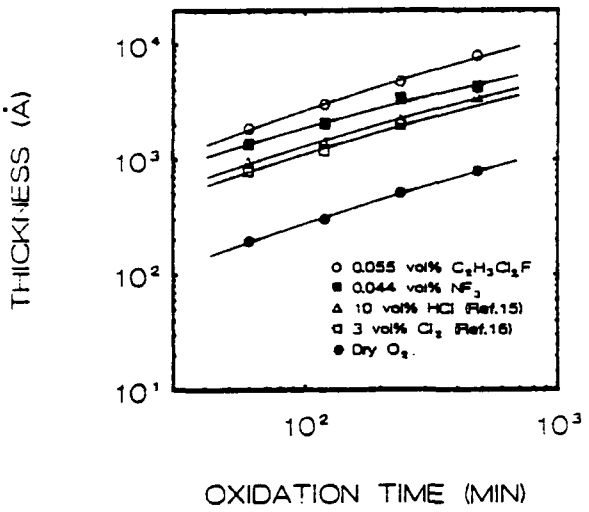

Fig. 1. Oxide thickness vs. oxidation time for the oxidation of lightly doped silicon in various gas ambients at 1000°C. The points represent the experimental data. Solid line is the least squares fit with the power of time.

tration was determined on a relative rather than on an absolute basis.

Results

Gas phase calculation results.—Table I contains results of the calculated composition of the gas phases at 900°C for the O_2/0.11 v/o $C_2H_3Cl_2F$ and the O_2/0.11 v/o NF_3 systems. The partial pressures of the various species are proportional to their concentrations in the system. At elevated oxidation temperatures, $C_2H_3Cl_2F$ dissociates to form many of the reaction products formed upon the dissociation of the commonly used chlorine additives, [*e.g.*, trichloroethylene ($C_2H_3Cl_3$) and trichloroethane (C_2HCl_3)]. Some of these reaction products, such as HCl, H_2O, or Cl_2, are known to enhance the growth rate (14). However, there is one compound that was unique to the $O_2/C_2H_3Cl_2F$ system, which was present in relatively large amounts, namely, hydrogen fluoride (HF). Since the chlorine compounds cannot account for the large observed increase in the oxidation rate, it was postulated that HF was the primary active species.

For the case of O_2/NF_3 system, it can be seen from the Table I that a significant amount of atomic fluorine (F) is present. However, it is also expected that residual

Table I. Composition of gas phase at 900°C with O_2/0.11 v/o $C_2H_3Cl_2F$ and O_2/0.11 v/o NF_3 system. (Ten ppm of H_2 added to each system considering the hydrocarbon impurities in the oxygen.)

$O_2/C_2H_3Cl_2F$ system		O_2/NF_3 system	
Chemical species	Partial pressure	Chemical species	Partial pressure
O_2	0.99×10^{0}	O_2	0.99×10^{0}
HCl	0.43×10^{-2}	F	0.51×10^{-2}
HF	0.22×10^{-2}	ONF	0.76×10^{-2}
CO_2	0.22×10^{-2}	N_2	0.71×10^{-2}
H_2O	0.28×10^{-4}	F_2	0.29×10^{-3}
Cl_2	0.22×10^{-4}	HF	0.99×10^{-4}
Cl	0.12×10^{-4}	FO_2	0.11×10^{-4}

amounts of moisture and hydrocarbons will provide some H_2 which will quickly give rise to HF in the furnace ambient. Thus, it is postulated that both F and HF readily form in either case and are the active species responsible for the increase in the oxidation rate. Similar simulated runs with other related compounds (various Freons, etc.) lead to essentially the same conclusions.

Oxidation results.—The fluorine oxidations were carried out by varying four parameters—oxidation temperature, time, fluorine concentration, and the type of fluorine additive. In Fig. 1, we plot oxide thickness *vs.* oxidation time for oxidations at 1000°C with 0.055 v/o $C_2H_3Cl_2F$ and 0.044 v/o NF_3 addition. These data were chosen so that a direct comparison with the published data for films grown in 10 v/o HCl and 3 v/o Cl_2 (15, 16) could be made. It is observed that the resultant oxide is thicker for films grown using the fluorine compounds despite the two orders of magnitude difference in the volume percent addition.

Figures 2a and b present oxide thickness *vs.* oxidation time data for increasing $C_2H_3Cl_2F$ concentration at 900° and 1000°C, respectively. It is seen that increasing the amount of $C_2H_3Cl_2F$ acts to enhance the oxidation rate. In Fig. 2b, for the case of 1000°C at the high concentrations (at ≥0.011 v/o) and longer times, represented by data shown with the dashed line, poorer quality oxides are observed, *i.e.*, the oxides have pinholes. This observation is consistent with the role of carbon as a nucleating agent for pinholes in the presence of HF.

Figures 3a and b present the comparable data of oxide thickness *vs.* oxidation time for increasing volume concentration of NF_3. It is found that the NF_3 species is also effective in enhancing the oxidation rate as can be expected from its chemistry. It should also be noted that contrary to the result of the above hydrocarbon source, optically clear pinhole free oxides result when using NF_3 over the entire

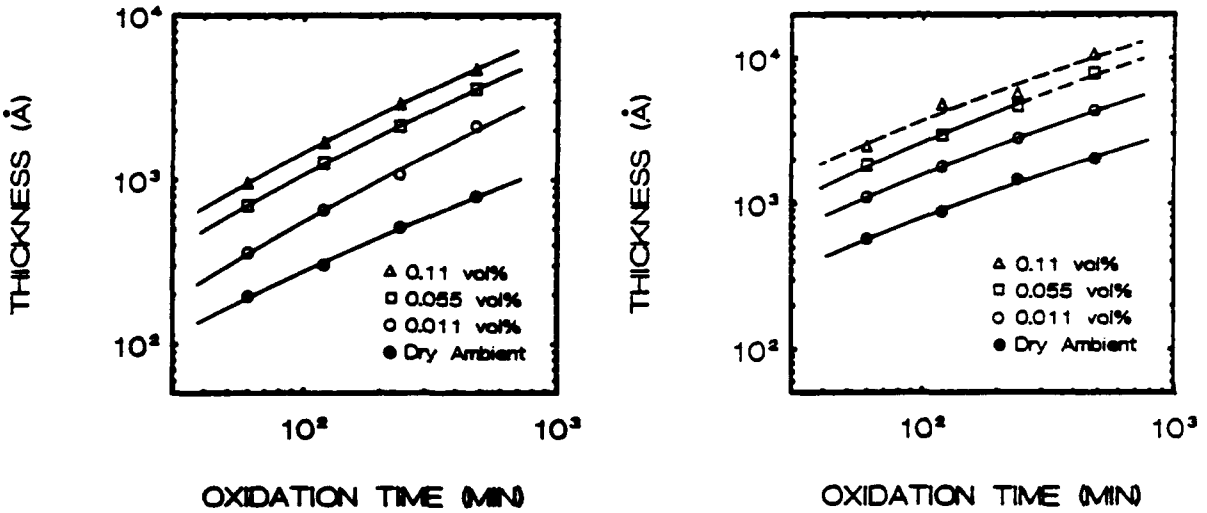

Fig. 2. Oxide thickness vs. oxidation time for the oxidation of (100) silicon in various $O_2/C_2H_3Cl_2F$ oxidation (a, left) at 900° and (b, right) at 1000°C. The points represent the experimental data. Solid line is the least squares fit with the power of time.

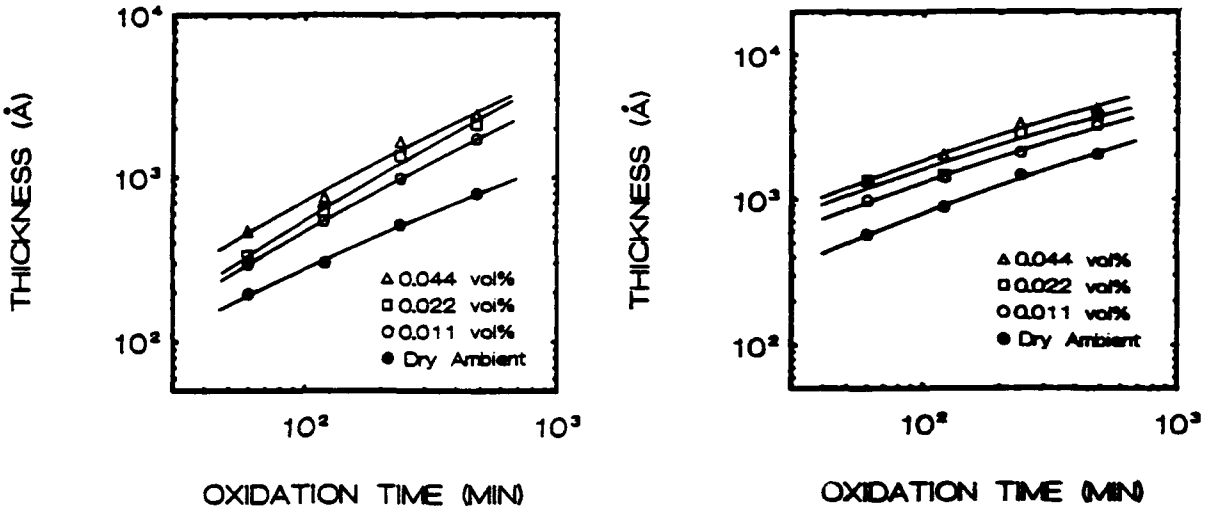

Fig. 3. Oxide thickness vs. oxidation time for the oxidation of (100) silicon in various O_2/NF_3 oxidation (a, left) at 900°C and (b, right) at 1000°C. The points represent the experimental data. Solid line is the least squares fit with the power of time.

concentration, oxidation time-temperature range of these studies.

The experimental data was treated in terms of the linear-parabolic model (10) and the more recently proposed power of time model (11, 12). The following two relationships were used to extract the appropriate parameters

$$X = a(t_g + t_o)^b \quad [1]$$

$$X = A\{[1 + 4B(t + \tau)/A^2]^{0.5} - 1\}/2 \quad [2]$$

where X is measured oxide thickness. For the power of time model, a and b are coefficient and exponent, respectively, while t_g and t_o are the oxidation times required to grow the final measured oxide and the pre-existing oxide. The constants a, b, and t_o were determined by least squares analysis. Since these oxidations were all performed at long oxidation time intervals, a simple least squares fit the data very well. The A and B in Eq. [2] are the constants in the linear-parabolic model, t is the oxidation time, and τ is a fitting parameter which accounts for initial rapid growth regime. The constants A and B were determined from X vs. $(t + \tau)/X$ plots. The fitting parameter τ was determined by the intersection of the extrapolated linear portion of the linear-parabolic model with the time axis. This extrapolation provided a constant value of the initial rapid growth of 180 + 20Å for all the data of these fluorine oxidations.

The resultant calculated constants for both these models are given in Table II and III. The solid line in Fig. 2 and Fig. 3 are the least squares fit with the power of time model. This fit was superior to the linear-parabolic model and therefore was used. As pointed out by Blanc (17) and others, reasonable physical models can lead to equivalent mathematical expression for the thickness as a function of time and that a large class of models[2] exhibit similar mathematical structure. The value of carrying forward analysis of the above two models is that the power of time model provides the best fit to the data while the linear-parabolic treatment ties back to the large body of data already published.

The enhanced oxidation rate for the oxides grown with increasing concentrations of fluorine compounds is readily evident from Fig. 2 and Fig. 3. When the data are compared to previously published results of the oxidation of 1-10 v/o HCl (15), several interesting differences are evident apart from the nature of the impurity. For all case of fluorine oxidation both the linear and parabolic constants increase with increasing fluorine concentration, whereas in the comparable HCl data only the parabolic rate constant increases over the full HCl concentration range. In the case of oxidation data at 900° and 1000°C, an almost order of magnitude increase occurs in these parameters in spite of the much lower fluorine concentration. As increasing amounts of NF_3 are added to the oxidation, the optical refractive index was found to decrease from 1.46 to 1.451. This leaves one to infer that the fluorine incorporation decreases the density of the oxide and also has an influence on the viscoelastic properties of the resultant oxide much as water vapor does. In fact, this correlates with some of the experience of workers in the area of silica optical fibers (18).

SIMS results.— Typical fluorine concentration *vs.* depth profiles for oxide films grown using $O_2/C_2H_3Cl_2F$ source are shown in Fig. 4 and Fig. 5, for the same v/o addition but at the extremes of the investigated temperature range. The

Table II. Effect of fluorine additive on the constants from the power of time model oxidation at 900° and 1000°C

T(°C)	Ambient	a	b	t_o (min)	Error
900°	Dry O_2	9.30	0.72	6.5	0.0008
	0.011 NF_3	46.77	0.66	1.6	0.0003
	0.022 NF_3	46.77	0.70	1.6	0.0097
	0.044 NF_3	63.09	0.64	5.0	0.0141
	0.011 $C_2H_3Cl_2F$	52.48	0.65	5.0	0.0022
	0.055 $C_2H_3Cl_2F$	107.15	0.56	5.0	0.0015
	0.11 $C_2H_3Cl_2F$	147.91	0.53	5.0	0.0013
1000°	Dry O_2	128.82	0.45	0.3	0.0034
	0.011 NF_3	131.82	0.50	35.0	0.0001
	0.022 NF_3	169.82	0.47	30.0	0.0239
	0.044 NF_3	338.84	0.36	30.0	0.0107
	0.011 $C_2H_3Cl_2F$	208.92	0.45	30.0	0.0029
	0.055 $C_2H_3Cl_2F$	213.79	0.51	24.0	0.0016

Table III. Effect of fluorine additive on the constants from the linear-parabolic models during oxidation at 900° and 1000°C

T(°C)	Ambient	$B(\mu m^2/h)$	$A/B(\mu m/h)$	$\tau(h)$
900°	Dry O_2	0.0021	0.0122	1.4
	0.011 NF_3	0.0047	0.0127	1.2
	0.022 NF_3	0.0059	0.0152	1.0
	0.044 NF_3	0.0081	0.0194	0.8
	0.011 $C_2H_3Cl_2F$	0.0258	0.0280	1.0
	0.055 $C_2H_3Cl_2F$	0.0438	0.0629	0.5
	0.11 $C_2H_3Cl_2F$	0.0724	0.0946	0.25
1000°	Dry O_2	0.0073	0.0709	0.4
	0.011 NF_3	0.0192	0.1053	0.4
	0.022 NF_3	0.0203	0.2203	0.4
	0.044 NF_3	0.0278	0.2530	0.4
	0.011 $C_2H_3Cl_2F$	0.0471	0.1162	0.2
	0.055 $C_2H_3Cl_2F$	0.1105	0.1162	0.1

[2] We acknowledge the suggestion made by the reviewer for this approach.

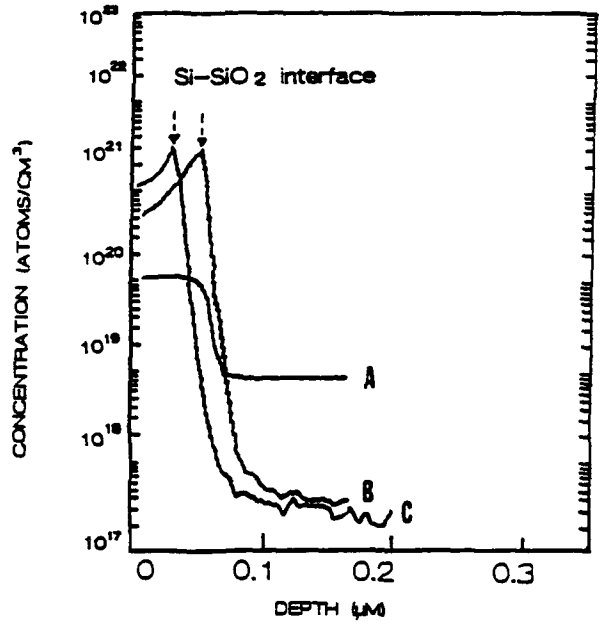

Fig. 4. Fluorine and oxygen profiles of an oxide grown at 800°C with 0.011 v/o $C_2H_3Cl_2F$ in O_2. A, oxygen profile; B, 8h and C, 2h.

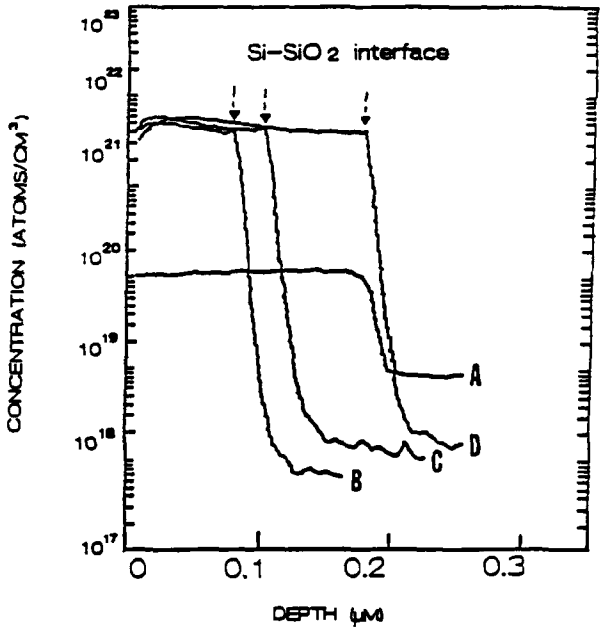

Fig. 6. Fluorine and oxygen profiles of oxides grown in different amounts of NF_3 addition at 900°C. A, oxygen profiles; B, 2h 0.011% NF_3; C, 2h 0.033% NF_3; D, 4h 0.022% NF_3.

oxygen signal is presented on an arbitrary scale to show the position of the interface as well as to calibrate the sputtering depth. Some of the data for the O_2/NF_3 oxidation are shown in Fig. 6 for NF_3 concentrations of 0.011, 0.022, and 0.033 v/o.

A comparison of the fluorine profiles show a consistent difference between the two sources. The fluorine profiles using $C_2H_3Cl_2F$ are characterized by a fluorine peak which moves with the silicon-oxide interface. The fluorine concentration is low at the surface, and increasing to a peak concentration at almost three-quarters of the oxide thickness where it remains more or less constant to the interface. In contrast to this, the oxides, grown using NF_3 are typified by the profiles shown in Fig. 6, namely, they exhibit a high uniform concentration of fluorine throughout the oxide as if the fluorine were tightly bonded into the oxide network and not mobile.

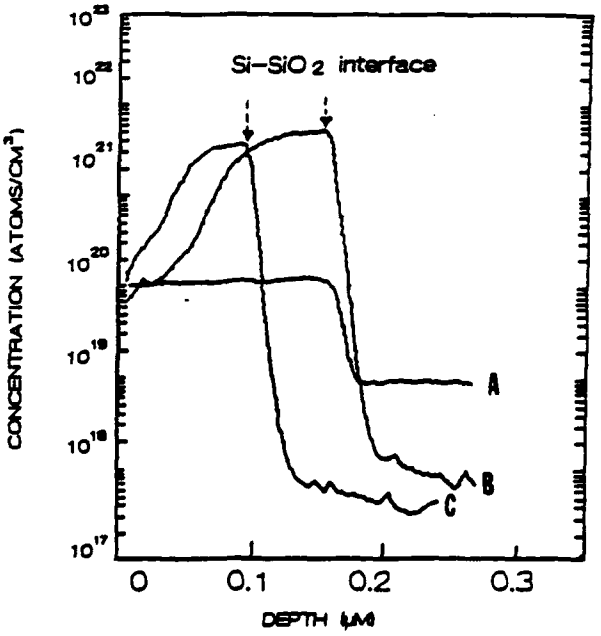

Fig. 5. Fluorine and oxygen profiles of an oxide grown at 1000°C with 0.011 v/o $C_2H_3Cl_2F$ in O_2. A, oxygen profiles; B, 2h; C, 1h.

Discussion

Gas-phase composition: Active fluorine species.—The SOLGAS calculation for fluorine compound additions provided a convenient guide in selecting potential sources and assessing the partial pressure of the resulting active species. Table I lists the species with the highest concentrations that are present during the oxidation at 900°C for each of the sources used in this study. These calculations showed that commonly used compounds such as C_2HCl_3 or $C_2H_3Cl_3$, when heated, will give similar active species (except for the fluorine-related species) as the $C_2H_3Cl_2F$ type source. Those findings are similar to those observed for HCl or chlorine oxidation (15) leading one to conclude that the essential difference in the enhanced oxidation rates is the presence of the high concentration of HF. However, when the concentration of this active species (HF) increases, especially in the presence of carbonaceous impurities, pinholes result.

When the NF_3-type source is used, it dissociates rapidly at elevated temperatures. Table I shows that an appreciable amount of F is present in the furnace which results in the enhanced oxidation rate. The presence of even small amounts of H_2 (between 0.000005 and 0.005 moles) affects the concentration of active species and forms HF. The results of such a simulation are shown in Fig. 7, where the active species are plotted as a function of temperature. It can be seen that for 0.005 v/o of H_2 an appreciable concentration of HF is formed throughout the entire temperature range. The HF concentration changes directly with v/o NF_3 added to the O_2 ambient if H_2 is present.

Thermal oxidation in the presence of fluorine.—The significant enhancement of the oxidation rate was achieved by small fluorine additions to the oxidation stream. In the case of a hydrogen bearing compound, some of the enhancement is due to the *in situ* formation of H_2O. This effect has been observed for the enhancement of oxidation which takes place using only hydrogen-chlorine compounds (such as HCl), but in no case is it of the same magnitude, as can be seen from the comparison of the growth curves in Fig. 1. From the comparison of the $O_2/C_2H_3Cl_2F$ system with the O_2/NF_3 system in the oxide thickness *vs.* time data, one can see that the presence of a significant

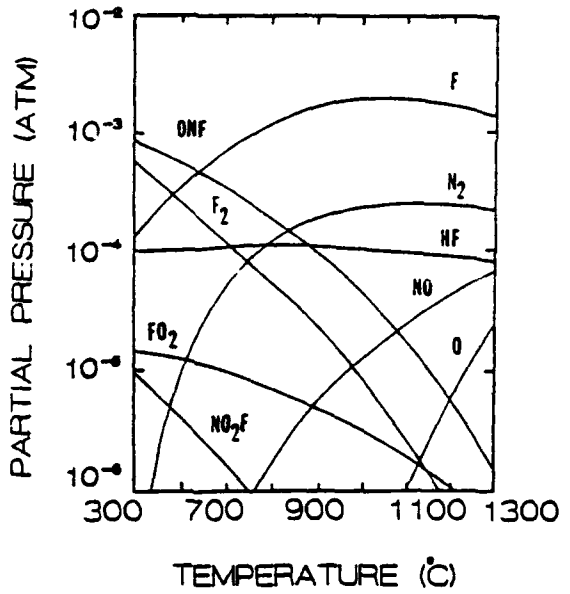

Fig. 7. Equilibrium partial pressure in N—F—O—H system vs. temperature. (Total pressure = 1 atm, NF_3 = 0.044 v/o and H_2 = 0.005 v/o.)

partial pressure of HCl and H_2O along with the HF aids in the enhancing the oxidation rate. The observation of pinholes at the higher temperatures and higher concentrations of $C_2H_3Cl_2F$ indicates that local etching occurs in competition with growth. In the same temperature and similar concentration ranges, with care, the NF_3 source results in optically clear and pinhole-free oxides. In this regard, it was reported that etching and growth occurs in the lower concentration range used in this work (4). However, Morita's data has been recently corrected (19) for underestimating the actual amounts of NF_3 by 9.7 times and now their results agree generally with our data. The remaining differences can be accounted for by recognizing that Morita *et al.* used a cold-wall quartz reactor with a halogen lamp heater *vs.* the standard hot-wall quartz oxidation system in this study. The presence of a large area of hot quartz has a strong influence on the attack of active species and their effective participation in the growth process.

The effect of fluorine additions on the model parameters is shown in Tables II and III for the linear-parabolic and power of time models. These parameters will be used to guide the understanding of the detailed processes that may be occurring. The assumptions and factors that relate interface reaction, diffusion, and solubility of oxidant in a comprehensive and complete theory are still under intense investigation (20, 21). The addition of chemical species to enhance the oxidation rate further complicates the development of a theoretical model. Several recently published articles have dealt with the relation of mechanism to the mathematical formulations used in this study. Following the work of Blanc (17), Wolters and Zegers-van Duynhoven (22) have analyzed the relationship between the power of time and the linear-parabolic expressions. They concluded that the Deal and Grove's linear-parabolic expression is an approximation to the power of time expression as suggested by Blanc and can be useful as a guide for technology. From their analysis, it can be seen that the "linear" and "parabolic" constants used in the Deal and Grove model are in reality only two terms of a series expression and the τ in their theory is added to compensate for the missing higher order terms. The larger the values of the parabolic and linear constants, the less important are the higher order terms and the smaller τ value added (22). Wolter and Zegers-van Duynhoven suggest an ionic space charge-limited growth mechanism for their growth model. However, the expression for oxide growth rate given by their Eq. [1] makes a correlation with the extracted parameters from this study difficult.

A mechanistic model for the power of time relationship has also been recently proposed by Nicollian and Reisman (23). In this model, they propose a surface reaction controlled mechanism driven by the generation of free volume through the volume expansion and the subsequent viscous flow in the oxidation process. The average viscosity of the oxide is time, temperature, and pressure dependent because the oxide undergoes oxide ring reconfiguration during growth, *i.e.*, the time dependent viscosity is the cause of a time dependent forward specific reaction coefficient. This model shows some of the characteristics of other models (24) but differs in its treatment of the time dependence of the viscosity, *i.e.*, it does not make the assumption that the oxide is a Maxwellian (viscoelastic) fluid. More to the point, this model involves the conversion of the Si lattice into Si—O—Si rings, and as such involves microscopic mechanisms through the power of time model exponent b. It is found that b varies from about 0.85 to 0.57 depending on the oxidation conditions at one atmosphere (11). In general, for a diffusion-limited oxidation, the value of b is expected to be 0.5. On the other hand, if strictly reaction-limited b should be equal to 1. Our data gives values varying between 0.7 and 0.5 with the b value generally decreasing with increasing concentrations of the fluorine additive. This indicates that even at low concentrations of fluorine b values are affected and are generally lower than those at 900°C for 1 atm dry oxidation. At 1000°C, all the b values determined in this study are at or below 0.5.

Looking at the parameters extracted from the linear-parabolic treatment, one can see an increase in both the parabolic and linear constants as a function of temperature and additive concentration. It is also shown that both the parameters associated with diffusion (B) as well as the linear rate constant (B/A) increase with fluorine additive concentration. As stated previously, the power of time gives a superior fit to the data and one measure of this is the larger values of τ needed in the linear-parabolic fit.

Several possibilities can be proposed for the effectiveness of fluorine as an oxidation enhancer. Flourine can act catalytically at the interface and competes with oxygen to form Si—F bonds (25) (based on electronegativity differences). This increases the available number of Si dangling bonds (analogous to the mechanism proposed for F etching of Si). This enhanced activity increases the reactivity at the interface and subsequently the growth rate of the oxidation. Fluorine can also effectively substitute for oxygen as a oxide network modifier and thus modify the structure, *i.e.*, open the structure to more readily allow ingress of the oxidant. This also directly relates to the change in the local stress and viscosity at the interface, and correlates with the lower index of refraction observed. Analysis of our data does not enable us to eliminate either of these mechanisms. A more complete mechanistic theory, especially, one that considers the chemical effect and oxide history on oxidation is still lacking. Such a theory would lead to specific experiments testing these mechanistic models.

Fluorine profiles in the oxide.—The fluorine concentration profiles determined by SIMS were found to have distinct differences depending on which chemical source was used, *i.e.*, whether large amounts of moisture forming impurities were present during the growth. The profiles that result from the oxides grown with $C_2H_3Cl_2F$ yield profiles peaked near the silicon-oxide interface. As the oxidation temperature increases the fluorine continues to peak and saturate at a high concentration, broadening from this position at an almost constant concentration before decreasing to the outside interface. This shaped profile is directly analogous to the profiles found for chlorinated oxides (26). This behavior can be explained by a replacement reaction proposed for chlorine and the critical role of hydroxyl (OH) species in this mechanism.

As the oxidation of $C_2H_3Cl_2F$ proceeds, a significant amount of water is generated and the bound fluorine can be weakened and replaced by OH groups. Continuing by the analogy to chlorinated oxide, one needs to postulate that a replacement reaction similar to

$$\equiv Si—F + H_2O \rightarrow Si—OH + HF \qquad [3]$$

occurs during the growth. This replacement reaction decreases the bonded fluorine concentration in the bulk oxide from the initial high concentration of bonded fluorine at the silicon-oxide interface. The mechanism outlined in Ref. (26) needs to be pursued as a possible detailed description of these fluorine profiles.

In contrast, the typical profiles obtained from the O_2/NF_3 oxidation behave in a markedly different way as can be seen from Fig. 6. Here, in the absence of a large amount of moisture, the fluorine is bonded into the oxide and remains at a high saturating concentration throughout the bulk. Insights into the behavior of NF_3 in oxides can be gleaned from work on optical fibers (27). In this case, fluorine can compete and isomorphously replace OH in the structure. It has been found that fluorine is thus randomly incorporated into the silica network in the form of silicon monofluoride sites $[Si(O^-)^3F]$ and silicon difluoride sites $[Si(O^-)^2F_2]$ (27). The Si—O—F complex is thermodynamically more stable than SiO_2. Thus the fluorine profiles in this case are expected to be more uniform throughout the bulk and limited by the solubility of fluorine in the oxide. Note that in the Ref. (27), no evidence was found for the formation of silicon trifluoride or silicon tetrafluoride (SiF_4), which would lead to a higher fluorine concentration at the interface.

Summary

It was shown that small additions of compounds containing fluorine such as $C_2H_3Cl_2F$ and NF_3 to a dry oxidation ambient enhanced the oxidation kinetics considerably. The enhanced kinetics indicate that diffusion through the already grown oxide as well as the reaction at the silicon-oxide interface was increased by the fluorine additives.

The crucial distinction between NF_3 and $C_2H_3Cl_2F$ in the chemistry is that $C_2H_3Cl_2F$ provides reactive fluorine and chlorine as well as water vapor. From the thermodynamic analysis of the oxidation ambient, it was determined that HF and F were the major active species for $O_2/C_2H_3Cl_2F$ oxidation and for O_2/NF_3 oxidation, respectively. Thus, during these oxidations, a local etching process competes with the growth process because of the presence of the HF. If this concentration exceeds a crucial amount, poor quality oxide results, in which pinholes and weakened structure have been observed.

It is also found that $C_2H_3Cl_2F$ oxides yield fluorine profiles which are peaked at the silicon-oxide interface. The peaks are sharp for the thinner oxides, and broader for thick oxides. For the NF_3 oxides, the fluorine profile is constant at a high concentration throughout the oxides. The incorporation behavior of fluorine into the growing oxide is based on the availability and competition between the hydroxyl group and the bonded fluorine for bridging sites in the oxides.

Acknowledgments

The authors gratefully acknowledge Dr. T. Kook for useful discussions in the course of this experiment. In addition, they would like to thank Dr. J. Parks for his contribution to this manuscript. This work was supported in part by the Army Research Office under grant DAAL 0388-K-0094 and by the Sherman Fairchild Foundation Fellowships.

Manuscript submitted June 23, 1988; revised manuscript received ca. Jan. 15, 1990.

Lehigh University assisted in meeting the publication costs of this article.

REFERENCES

1. R. J. Kriegler, Y. G. Cheng, and D. R. Colton, *This Journal*, **119**, 388 (1979); R. J. Kriegler, Y. G. Cheng, and D. R. Colton, U.S. Pat. 3,692,571 (1972).
2. J. Monkowski, *Solid State Technol.*, 58 (July 1979); *ibid.*, 113 (Aug. 1979).
3. P. F. Schmidt, R. J. Jaccodine, C. H. Wolowodiuk, and T. Kook, *Mat. Lett.*, **3**, 235 (1985).
4. M. Morita, T. Kub, T. Ishihara, and M. Hirose, *IEDM Tech. Dig.*, 144 (1984).
5. Y. Nishioka, Y. Ohji, K. Mukai, T. Sugano, Y. Wang, and T. P. Ma, *Appl. Phys. Lett.*, **54**, 1127 (1989).
6. U. S. Kim and R. J. Jaccodine, *ibid.*, **48**, 1201 (1986).
7. U. S. Kim, T. Kook, and R. J. Jaccodine, *This Journal*, **135**, 270 (1988).
8. E. F. da Silva, Jr., Y. Nishioka, and T. P. Ma, *IEDM Tech. Dig.*, 848 (1987).
9. G. Erikssoon, *Acta Chem. Scand.*, **26**, 2651 (SOLGAS Program) (1971).
10. B. E. Deal and A. S. Grove, *J. Appl. Phys.*, **36**, 3770 (1965).
11. A. Reisman, E. H. Nicollian, C. K. Williams, and C. J. Merz, *J. Electron. Mater.*, **16**, 45 (1987).
12. R. Doremus and A. Szewczyk, in "Silicon Nitride and Silicon Dioxide Thin Insulating Films," (PV 87-10) V. J. Kapoor and K. T. Hankins, Editors, p. 350, The Electrochemical Society Softbound Proceedings Series, Pennington, NJ (1987).
13. D. R. Stull and H. Prophet, JANAF Thermochemical Tables, 2nd ed., NSRDS-NBS37 (1971).
14. R. E. Tressler, J. Stach, and D. M. Metz, *This Journal*, **124**, 607 (1977).
15. D. W. Hess and B. E. Deal, *ibid.*, **124**, 735 (1977).
16. B. E. Deal, D. W. Hess, J. D. Plummer, and C. P. Ho, *ibid.*, **125**, 339 (1978).
17. J. Blanc, *Philos. Mag.*, **55**, 685 (1987).
18. P. D. Lazay and A. D. Pearson, *IEEE J. Quantum Electron.*, **QE-18**, 504 (1982).
19. S. Aritome, M. Morita, T. Tanaka, and M. Hirose, *Appl. Phys. Lett.*, 981 (1987).
20. Oxidation Workshop, *Philos. Mag.*, 55 (1987).
21. "The Physics and Chemistry of SiO_2 and Si-SiO_2 Interface," C. R. Helms and B. E. Deal, Editors, Plenum Press, New York (1988).
22. D. R. Wolters and A. T. A. Zegers-van Duynhoven, *J. Appl. Phys.*, **65**, 5126 (1989); D. R. Wolters and A. T. A. Zegers-van-Duynhoven, *ibid.*, **65**, 5133 (1989).
23. E. H. Nicollian and A. Reisman, *J. Electron. Mater.*, **17**, 263 (1988).
24. E. A. Irene, *J. Appl. Phys.*, **54**, 5416 (1983).
25. M. Seel and P. S. Bagus, *Phys. Rev. B.*, **28**, 2023 (1983).
26. Y. D. Sheu, S. R. Butler, F. J. Feigl, and C. W. Magee, *This Journal*, **133**, 2137 (1986).
27. T. M. Duncan, D. C. Douglass, R. Csencsits, and K. L. Walker, *J. Appl. Phys.*, **60**, 130 (1986).

Reprinted from JOURNAL OF THE ELECTROCHEMICAL SOCIETY
Vol. 137, No. 7, July 1990
Printed in U.S.A.

APPENDIX B

Electron injection studies on fluorine-implanted oxides

Dunxian D. Xie and Donald R. Young
Sherman Fairchild Center, Lehigh University, Bethlehem, Pennsylvania 18015

(Received 21 December 1990; accepted for publication 23 May 1991)

The effect of fluorine on electron trapping in SiO_2 films has been studied by avalanche electron injection. Samples are prepared by 25-keV fluorine implantation into dry oxides followed by a 1000 °C N_2 ambient anneal. Bulk electron traps with capture cross sections on the order of 10^{-17}–10^{-19} cm^2, which are not due to implantation damage, are filled by avalanche electron injection. An optimum dosage of fluorine implantation to suppress the so-called turnaround effect during avalanche injection exists. This suggests that fluorine might passivate slow interface donor states or reduce bulk hydrogen diffusion. The observation that high-temperature (120 °C) injection can eliminate most fast and slow interface states for conventional oxides is also true for fluorinated oxides. Our results indicate an enhanced generation of fast donor states for oxides containing fluorine. These states contribute a positive charge when the Fermi level is in the lower portion of the band gap.

I. INTRODUCTION

As metal-oxide-semiconductor (MOS) devices are widely used in modern very large scale integration (VLSI) technology, many investigators have been trying to improve the qualities of oxides by various approaches. The use of fluorine in the SiO_2 films, although it is still in research stages, is one of the possibilities to make good quality devices. Fluorine reduces the generation of interface states when it is properly introduced into SiO_2. Nishioka *et al.*[1–3] observed the densities of radiation-induced oxide charge and interface states were reduced when small quantities of fluorine were added before or during dry oxidation. They explained their results by the oxide bond strain gradient model which suggests that the fluorinated oxides, with a smaller strain gradient, reduce the migration of radiation-induced defects to the Si-SiO_2 interface. Wright *et al.*[4–6] studied the effect of fluorine on SiO_2 via F^+ (fluorine ion) implantation using different doses, ranging from 10^{12} to 10^{16} cm^{-2}, at 40 and 90 keV. Physical ion damage was observed after high-field current injection for their F^+-implanted oxides even after annealing at 900–1000 °C. Their results also indicated a decrease in the charge to breakdown for the highest dose (10^{16} cm^{-2}) F^+ implantation used.[4] Charge to breakdown means the integrated injected charge per unit area from a virgin sample to a sample showing a resistive characteristic.

In this paper, we will discuss the electron trapping phenomena of fluorinated oxides by the avalanche injection technique. Both bulk and interface traps were studied mainly for low-energy (25 keV) F^+-implanted MOS capacitors. The results of fluorinated oxides were compared with those of nonimplanted and Ne^+ (neon ion) implanted samples.

II. SAMPLE PREPARATION AND EXPERIMENTS

Silicon wafers, ⟨100⟩ B-doped *p*-type, 0.1–0.2 Ω cm are used for our experiments. The oxide is grown in a dry oxidation furnace at 1000 °C (dry oxygen, 2 l/min). The samples are implanted with F^+ or Ne^+ at low energy (25 keV) on half of each wafer. The other half is the control sample used for comparison. The fluorine doses are selected in the range from 10^{13} to 10^{15} cm^{-2}. After implantation, the samples are annealed for 30 min in a N_2 (nitrogen) ambient at 1000 °C to remove the physical damage resulting from the implantation. Aluminum dots (area: 7×10^{-3} cm^2) are deposited in a vacuum chamber with low sodium contamination to define the gate of MOS capacitors for electrical measurements. Finally, the devices receive a 400 °C, 30-min post-metal anneal in a forming gas (20% H_2/80% N_2) mixture.

The fluorine distribution in the oxides is profiled using secondary-ion-mass spectrometry (SIMS). Electron injection current is induced in the MOS devices via the avalanche injection technique.[7] During the measurement, the average avalanche current density, monitored by a Keithley 616 electrometer, is set at a value of 2–2.3 $\times 10^{-5}$ A/cm^2. The measuring equipment has been previously described by Young *et al.*[8,9] The constant current injection is achieved by a 150-kHz saw-tooth wave form. Automatic data acquisition enables us to measure the flatband and midgap voltage shifts at room and elevated temperatures.

Both 1-MHz high-frequency and quasistatic *C-V* data are taken by a 410 *C-V* plotter (Princeton Applied Research) and Keithley 602 electrometer, respectively. By comparing *C-V* curves before and after avalanche injection, we are able to obtain the information containing the bulk and interface characteristics due to the effects of avalanche electron injection.

III. RESULTS

The results of SIMS measurements of F^+-implanted oxides after a 30-min N_2 anneal at 1000 °C are shown in Fig. 1. These samples were implanted with different doses, ranging from 10^{13} to $10^{1\cdot}$ F^+/cm^2 at 25 keV as mentioned above. The peak positions are in the oxide and only 40–50 Å away from the Si-SiO_2 interface. When the dose is increased to 10^{15} F^+/cm^2, an additional shoulder appears towards the bulk of the oxide. This effect is likely due to

 0021-8979/91/052755-05$03.00

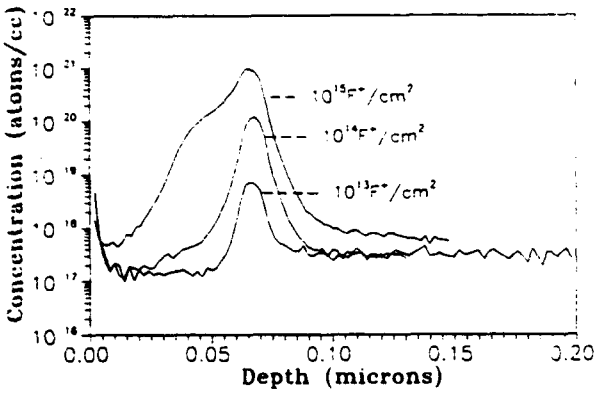

FIG. 1. SIMS profiles of fluorine implantation (25 keV) in oxides (d_{ox} = 700 Å), after a N_2 anneal at 1000 °C for 30 min.

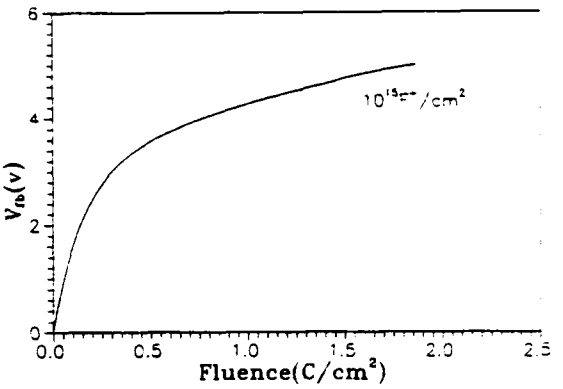

FIG. 3. Avalanche electron injection at 120 °C for fluorinated oxide (dose: 10^{15} F^+/cm^2; current density: 2 × 10^{-5} A/cm²; d_{ox} = 825 Å) showing no turnaround effect.

the enhanced diffusion of fluorine species at high concentrations above 10^{20} cm^{-3}.

The electron injection characteristic is studied by monitoring the flatband voltage shifts versus injection time or fluence for different devices. Figure 2 shows the comparison of nonimplanted (control) with F^+-implanted (fluorinated) samples with the injecting current density of 2 × 10^{-5} A/cm². Fluorinated samples have larger flatband voltage shifts than those of the control sample. Almost all the curves show a turnaround effect when the fluence becomes 0.2–0.8 C/cm² except for the sample with an implant dose of 10^{14} F^+/cm^2. The positive flatband voltage shift results from the negative charge trapped in the oxide. The turnaround effect is due to a positive charge that slowly builds up and compensates the negative charge in the oxides after a certain period of time of avalanche electron injection. This effect of the anomalous positive charge has been discussed in previous papers[10–12] and explained as resulting from donorlike slow states near the Si-SiO_2 interface. The optimum implant dose of 10^{14} F^+/cm^2 eliminates the buildup of the anomalous positive charge near the Si-SiO_2 interface.

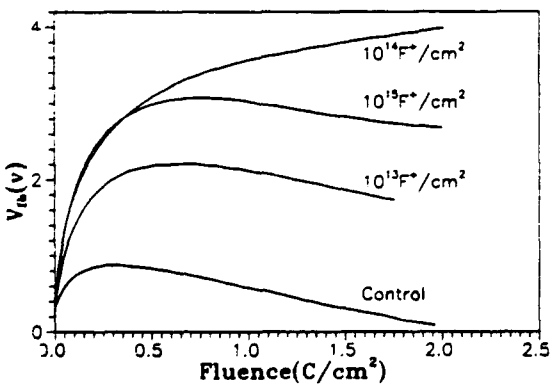

FIG. 2. Avalanche electron injection curves of control and fluorinated oxides at room temperature (d_{ox} = 600 Å; current density: 2 × 10^{-5} A/cm²) showing turnaround effect.

Another way of eliminating the turnaround effect is to perform the avalanche injection at 120 °C as reported in the literature.[8] As we can see in Fig. 3 for the sample with a dose of 10^{15} F^+/cm^2, the flatband voltage shift does not show the turnaround effect. The corresponding high-frequency and quasistatic *C-V* curves before and after the injection at both room temperature and 120 °C with a fluence of 2 C/cm² are shown in Fig. 4. In Fig. 4(a) we can see that the high-frequency *C-V* curve shows a stretch out after room-temperature injection and the bulk trapping effect is not easily estimated because of the buildup of the anomalous positive charge near the Si-SiO_2 interface. However, the high-frequency *C-V* curve becomes nearly parallel to the initial one after the injection at 120 °C. This enables us to determine *C-V* shift due to bulk electron trapping. In Fig. 4(b) the quasistatic *C-V* curve after the injection at 120 °C is significantly deeper than the one after room-temperature injection. This means that the generation of interface states is obviously reduced for elevated temperature injection.

In order to compare the physical damage due to implantation, we have implanted neon instead of fluorine with the results shown in Fig. 5. All of these samples received a N_2 anneal at 1000 °C for 30 min after implantation or after oxidation for the nonimplanted sample. The flatband voltage shifts of the Ne^+-implanted sample after electron injection are comparable to the nonimplanted control sample. These results indicate that physical damage does not play an important role in trapping electrons as a result of the annealing treatment we have used. We therefore conclude the additional flatband voltage shift of fluorinated samples during electron injection is not caused by physical damage resulting from the implantation. Our results are not the same as the observation of Wright and co-workers.[4,5] They attributed the negative flatband voltage shift during Fowler–Nordheim injection to the physical damage of F^+ and Ne^+ implantation; however, our results did not indicate damage for the Ne^- implanted sample after annealing. The flatband voltage shifts of

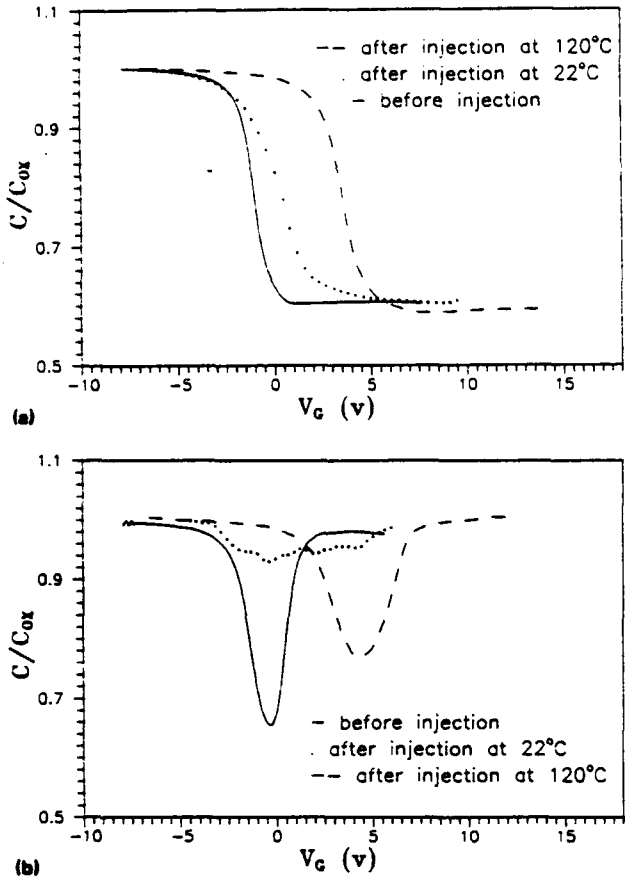

FIG. 4. (a) High-frequency C-V curves before and after avalanche injection (current density: 2×10^{-5} A/cm^2; dose:10^{15} F$^+$/cm^2; d_{ox} = 825 Å). (b) Quasistatic C-V curves before and after avalanche injection (current density: 2×10^{-5} A/cm^2; dose: 10^{15} F$^+$/cm^2; d_{ox} = 825 Å).

F$^+$- and Ne$^+$-implanted samples we observed were positive during avalanche injection.

We have also observed a larger stretch out in the C-V characteristic of our fluorinated oxides than that of control samples. This suggests the possibility of a relatively large effect on our flatband voltage measurements due to inter-

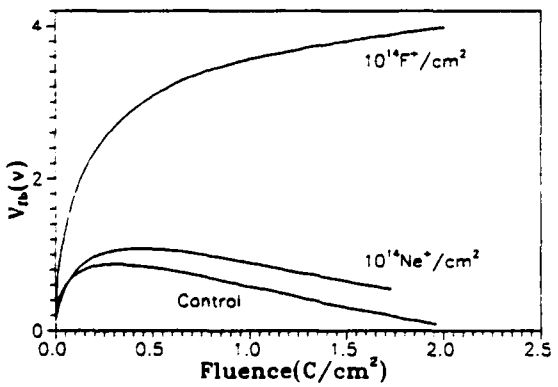

FIG. 5. The difference of flatband voltage shifts of control, neon- and fluorine-implanted oxides (d_{ox} = 600 Å). The implantation was followed by a N_2 anneal at 1000 °C for 30 min.

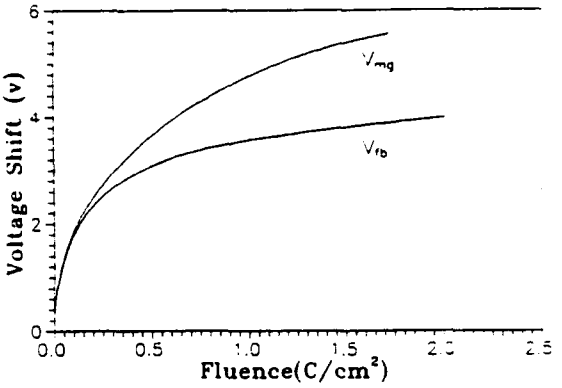

FIG. 6. Avalanche electron injection data showing the difference between midgap (V_{mg}) and flatband (V_{fb}) voltage shifts of the fluorinated oxide (dose: 10^{14} F$^+$/cm^2; d_{ox} = 600 Å).

face state generation. Following the suggestion of Lai and Young,[10] that the measurements be made at midgap to eliminate the effect of the interface state charge, we have obtained the results shown in Fig. 6 for samples with 10^{14} F$^+$/cm^2. As the midgap is usually the point that is less sensitive to the interface states, this difference characterizes interface state generation in these fluorine-implanted oxides after avalanche electron injection. We will discuss this phenomenon in the following section.

In analyzing the data of avalanche electron injection, we have obtained capture cross sections and trap densities of various electron trapping centers via measuring midgap voltage shifts for both control and F$^+$-implanted samples, as shown in Table I. The calculation method we used here is the one described in Young's previous paper.[9] The initial experimental curve of voltage shift versus fluence is fitted exponentially for different fluence regions. The magnitude of the exponentials is related to the trap density and the time constant is related to the trap cross section. The smallest cross-section trap is extracted first using the results for the largest fluences. The exponential due to the above trap is subtracted from the original data and the resultant used to characterize the next larger trap. This procedure continues until all the traps are extracted from the initial experimental curve. These exponentials are subtracted from the original data and the results are plotted to see if a good overall fit has been obtained. We measured

TABLE I. Capture cross section and trap density of nonimplanted and fluorine-implanted oxides.

Sample	Trap No.	Cross section $\sigma(10^{-18}$ cm^2)	Trap density $N_T(10^{11}$ cm^{-2})
Nonimplanted	1	1.83	2.31
(midgap)	2	0.11	3.63
10^{14}F/cm^2 (F18)	1	33.20	0.91
(midgap)	2	2.78	4.04
	3	0.24	15.10

three different dots on each wafer. The variations involved in cross sections were around 10%.

We can see from the table that the trap with a cross section of 3.32×10^{-17} cm^2 does not appear in control samples and fluorine does not create any larger traps than the above one. This might be an additional electron trap due to fluorine. Finally, in midgap measurements, two trapping centers with capture cross sections of 2.44×10^{-19} and 2.78×10^{-18} cm^2 become dominant as seen in the table for their higher trap densities. The reason we use midgap results instead of flatband results will be discussed in the following section.

IV. DISCUSSION

Based on above results, we have observed that fluorine implantation introduces new electron traps.

First, in examining current injection data of nonimplanted, Ne^+-implanted, and F^+-implanted samples, we found that physical damage resulting from the implantation is largely annealed out by our 1000 °C N_2 heat treatment. However, fluorine can react with silicon atoms in the oxide when it is implanted. It may cleave Si-O bonds to form Si-F bonds or gaseous compounds SiF_3 (Ref. 13) and leave the oxide with a more open structure. When electrons are injected into this oxide, the open structure may act as electron traps to cause the additional flatband voltage shift.

Second, the turnaround phenomenon during avalanche electron injection disappears for the sample with a F^+-implanted dose of 10^{14} cm^{-2}. From calibrated SIMS measurements, this dose corresponds to the fluorine concentration with a peak close to 10^{20} cm^{-3} near the Si-SiO_2 interface. Excess or smaller amount of the F^+ implant dose fails to eliminate the turnaround phenomenon.

The turnaround effect during avalanche electron injection for conventional oxides was discussed by Feigl *et al.*[14] years ago. The model they proposed was that atomic hydrogen released from water traps in the oxide diffuses to the Si-SiO_2 interface. This neutral species could further release an electron at the interface to build up the anomalous positive charge. It was also considered to be a donor-like slow interface state[10] because it only built up with long-time constants during current injection and could be charged and discharged by the application of a moderate electric field but does not respond during the usual C-V measurements. For the F^+-implanted sample with a dose of 10^{14} cm^{-2}, this turnaround effect does not exist. Suppose the atomic hydrogen diffuses to the Si-SiO_2 interface. It might form H—F bonds if there are enough fluorine ions near the interface. Thus, less positive charge builds up and the flatband voltage shift is increased. A dose of 10^{13} F^+/cm^2 does not seem to have enough fluorine to passivate the hydrogen based on the above argument. Whether the high-concentration ($>10^{20}$ F^+/cm^3) diffusion observed in SIMS profile accounts for the turnaround effect of the high-dose (10^{15} F^+/cm^2) fluorine-implanted oxides remains to be understood. Although we do not know exactly what chemical reaction is involved in eliminating the turnaround effect by fluorine implantation, it is worth noticing that an optimum dose does exist. This result from avalanche injection is analogous to what da Silva and coworkers found in the radiation-induced effect.[1] They also showed that an optimum amount of fluorine exists to minimize the radiation-induced interface trap density.

The process of interface state generation during electron injection is somewhat complicated. Both fast and slow states are generated at and in the vicinity of the Si-SiO_2 interface along with the bulk charge trapping in the oxide. The high-frequency C-V curve after injection will show a stretch out mainly due to the fast interface states since slow states are not sensitive to the stretch out but only result in a rigid shift in C-V ramp.[10] Thus, measuring the flatband voltage shift gives us the total trapping effect both near the interface and in the bulk of the oxide, whereas the midgap voltage shift primarily characterizes the bulk trapping effect since the interface states are not charged at this point. Therefore the data of capture cross sections of bulk trapping should be extracted from the midgap measurement rather than the flatband measurement. The difference between midgap and flatband shifts characterizes the generation of interface donor states that have a positive charge when the Fermi level is close to the valence band of the silicon but become discharged as the Fermi level moves to midgap.

In addition to the interface effect, fluorinated oxides also contain bulk electron traps with cross sections on the order of 10^{-17} cm^2. The neutral trap with the cross section of 2.78×10^{-18} cm^2 is larger than the usual water trap ($\sim2\times10^{-18}$ cm^2) in the conventional oxides. Another electron trap with a cross section of 2.44×10^{-19} cm^2 is twice as large as the one on the same order (1.11×10^{-19} cm^2) in the control sample. These traps might be created by the open structure of fluorinated oxides. However, fluorine does not seem to create any Coulombic traps or other neutral traps with cross sections larger than the order of 10^{-17} cm^2. It would be expected that only the larger capture cross-section traps would be of concern to device designers.

V. CONCLUSION

We have studied fluorinated samples by low-energy (25 keV) ion implantation. SIMS profiles show that the fluorine peaks are in the same spatial position after postoxidation anneal in N_2 ambient at 1000 °C and are close to the Si-SiO_2 interface. The high-dose (10^{15} cm^{-2}) fluorine profile has a shoulder going into the bulk oxide. This indicates a concentration-enhanced diffusion. Our electrical measurements indicate that, after avalanche injection, fluorinated oxides have additional bulk electron traps that are not due to implantation damage. The generation of interface donor states in fluorinated oxides could be annealed out during avalanche injection at 120 °C. Finally, an optimum dosage (10^{14} cm^{-2}) of fluorine implantation exists to suppress the turnaround effect during avalanche electron injection.

ACKNOWLEDGMENTS

The work is supported by a grant from Defence Nuclear Agency (DNA). We would like to thank Fred Stevie of AT&T Bell Labs, Allentown, PA for valuable SIMS measurements. We are indebted to Professor Ralph Jaccodine of Lehigh University whose long standing interest in the effect of fluorine has stimulated our work in this field. We also wish to thank Mr. Saikumar Vivekanand and Dr. Jeffrey Parks of the Sherman Fairchild Lab of Lehigh University for the help in making samples for our measurements.

[1] E. F. da Silva, Jr., Y. Nishioka, and T. P. Ma, IEEE Trans. Nucl. Sci. NS-34, 1190 (1987).
[2] Y. Nishioka, E. F. da Silva, Jr., Y. Wang, and T. P. Ma, IEEE Electron Device Lett. EDL-9, 38 (1988).
[3] Y. Nishioka, Y. Ohji, K. Mukai, T. Sugano, Y. Wang, and T. P. Ma, Appl. Phys. Lett. 54, 1127 (1989).
[4] P. J. Wright and K. C. Saraswat, IEEE Trans. Electron Devices ED-36, 879 (1989).
[5] P. J. Wright, M. Wong, and K. C. Saraswat, IEDM Tech. Dig., 574 (1987).
[6] P. J. Wright, N. Kasai, S. Inoue, and K. C. Saraswat, IEEE Electron Device Lett. EDL-10, 347 (1989).
[7] E. H. Nicollian and C. N. Berglund, J. Appl. Phys. 41, 3052 (1970).
[8] D. R. Young, E. A. Irene, D. J. DiMaria, R. F. Dekeersmaecker, and H. Z. Massoud, J. Appl. Phys. 50, 6366 (1979).
[9] D. R. Young, J. Appl. Phys. 52, 4090 (1981).
[10] S. K. Lai and D. R. Young, J. Appl. Phys. 52, 6231 (1981).
[11] C. Sah, J. Y. Sun, and J. J. Tzou, J. Appl. Phys. 54, 944 (1983).
[12] C. Sah, J. Y. Sun, and J. J. Tzou, J. Appl. Phys. 54, 2547 (1983).
[13] F. G. Kuper, J. Th. M. De Hosson, and J. F. Verway, J. Appl. Phys. 60, 985 (1986).
[14] F. J. Feigl, D. R. Young, D. J. Di Maria, S. Lai, and J. Calise, J. Appl. Phys. 52, 5665 (1981).

DISTRIBUTION LIST

DNA-TR-92-12

DEPARTMENT OF DEFENSE

ASSISTANT TO THE SECRETARY OF DEFENSE
ATTN: EXECUTIVE ASSISTANT

DEFENSE ADVANCED RSCH PROJ AGENCY
ATTN: ASST DIR ELECTRONIC SCIENCES DIV
ATTN: R REYNOLDS

DEFENSE ELECTRONIC SUPPLY CENTER
ATTN: DESC-E

DEFENSE INTELLIGENCE AGENCY
ATTN: DIW-4
ATTN: DT-1B

DEFENSE NUCLEAR AGENCY
ATTN: RAEE TREE
2 CYS ATTN: TITL

DEFENSE TECHNICAL INFORMATION CENTER
2 CYS ATTN: DTIC/FDAB

DNA PACOM LIAISON OFFICE
ATTN: DNALO

FIELD COMMAND DEFENSE NUCLEAR AGENCY
ATTN: FCPF R ROBINSON

FIELD COMMAND DEFENSE NUCLEAR AGENCY
ATTN: FCNM
2 CYS ATTN: FCTT W SUMMA

JOINT DATA SYSTEM SUPPORT CTR
ATTN: C-330
ATTN: JNSV

STRATEGIC AND THEATER NUCLEAR FORCES
ATTN: DR E SEVIN

DEPARTMENT OF THE ARMY

HARRY DIAMOND LABORATORIES
ATTN: SLCHD-NW-RP
ATTN: SLCHD-NW-TN
ATTN: SLCHD-NW-TS

U S ARMY MISSILE COMMAND
ATTN: AMCPM-HA-SE-MS

U S ARMY NUCLEAR & CHEMICAL AGENCY
ATTN: MONA-NU DR D BASH

U S ARMY RESEARCH OFFICE
ATTN: R GRIFFITH

U S ARMY STRATEGIC DEFENSE CMD
ATTN: CSSD-SA-E
ATTN: CSSD-SD-A

U S ARMY STRATEGIC DEFENSE COMMAND
ATTN: CSSD-SL

U S MILITARY ACADEMY
ATTN: LTC AL COSTANTINE

USAISC
ATTN: ASOP-DO-TL

DEPARTMENT OF THE NAVY

DEPARTMENT OF THE NAVY
ATTN: A NEWHOUSE NAVSEA 081

NAVAL AIR SYSTEMS COMMAND
ATTN: AIR-536T

NAVAL ELECTRONICS ENGRG ACTVY, PACIFIC
ATTN: CODE 250

NAVAL POSTGRADUATE SCHOOL
ATTN: CODE 1424 LIBRARY

NAVAL RESEARCH LABORATORY
ATTN: CODE 4600 D NAGEL
ATTN: CODE 4613 A B CAMPBELL

NAVAL SURFACE WARFARE CENTER
ATTN: CODE H21 F WARNOCK
ATTN: CODE H23 R SMITH

NAVAL SURFACE WARFARE CENTER
ATTN: CODE H-21

NAVAL TECHNICAL INTELLIGENCE CTR
ATTN: LIBRARY

NAVAL WEAPONS EVALUATION FACILITY
ATTN: CLASSIFIED LIBRARY

NAVAL WEAPONS SUPPORT CENTER
ATTN: CODE 6054 D PLATTETER

STRATEGIC SYSTEMS PROGRAM
ATTN: JIM HOWARD

DEPARTMENT OF THE AIR FORCE

AERONAUTICAL SYSTEMS DIVISION
ATTN: ASD/ENSS

AIR FORCE CTR FOR STUDIES & ANALYSIS
ATTN: AFSAA/SAKI

AIR UNIVERSITY LIBRARY
ATTN: AUL-LSE

OGDEN AIR LOGISTICS CENTER
ATTN: OO-ALC/LMIM
ATTN: OO-ALC/MMDEC HARDNESS CONTROL

PHILLIPS LABORATORY
ATTN: NTC M SCHNEIDER
ATTN: NTCTD
ATTN: PL/VTE
ATTN: PL/VTEE S SAMPSON

ROME LABORATORY
ATTN: RBR

ROME LABORATORY
ATTN: ESR

UNITED STATES STRATEGIC COMMAND
ATTN: J 63

WRIGHT RESEARCH & DEVELOPMENT CENTER
ATTN: AFWAL/ELE
ATTN: WRDC/MTE

3416TH TECHNICAL TRAINING SQUADRON (ATC)
ATTN: TTV

DEPARTMENT OF ENERGY

DEPARTMENT OF ENERGY
ALBUQUERQUE OPERATIONS OFFICE
ATTN: NESD

LAWRENCE LIVERMORE NATIONAL LAB
ATTN: L-156 J YEE
ATTN: L-84 G POMYKAL
ATTN: W ORVIS

LOS ALAMOS NATIONAL LABORATORY
ATTN: E LEONARD

SANDIA NATIONAL LABORATORIES
ATTN: DR T F WROBEL DIV 9341
ATTN: L D POSEY DIV 9351
ATTN: ORG 2146 T A DELLIN
ATTN: ORG 2535 F SEXTON
ATTN: P WINKUR DIV 1332
ATTN: 1332 P WUNOKUR
ATTN: 2140 J WOODARD

OTHER GOVERNMENT

CENTRAL INTELLIGENCE AGENCY
ATTN: OSWR/NED
ATTN: OSWR/STD/MTB

DEPARTMENT OF TRANSPORTATION
ATTN: ARD-350

NASA
ATTN: CODE 100.0 DR JAMES TRAINOR
ATTN: CODE 313 V DANCHENKO
ATTN: CODE 724.0 M JHABVALA
ATTN: CODE 900 E STASSINOPOULOS

NATIONAL INSTITUTE OF STANDARDS & TECHNOLOGY
ATTN: P ROITMAN

DEPARTMENT OF DEFENSE CONTRACTORS

ADVANCED RESEARCH & APPLICATIONS CORP
ATTN: R ARMISTEAD

AEROSPACE CORP
ATTN: A AMRAM
ATTN: C RICE
ATTN: D SCHMUNK
ATTN: K G HOLDEN
ATTN: M HOPKINS
ATTN: N SRAMEK
ATTN: P BUCHMAN
ATTN: R KOGA

ALLIED-SIGNAL, INC
ATTN: DOCUMENT CONTROL

AMPEX CORP
ATTN: B RICKARD
ATTN: K WRIGHT

ANALYTIC SERVICES, INC (ANSER)
ATTN: A HERNDON
ATTN: A SHOSTAK

BDM INTERNATIONAL INC
ATTN: D WUNSCH

BOEING CO
ATTN: A JOHNSTON
ATTN: M ANAYA
ATTN: ROS WOOD
ATTN: D EGELKROUT
ATTN: O MULKEY

BOOZ-ALLEN & HAMILTON, INC
ATTN: D VINCENT
ATTN: L ALBRIGHT

CALIFORNIA INSTITUTE OF TECHNOLOGY
ATTN: C BARNES

CALSPAN CORP
ATTN: R THOMPSON

CHARLES STARK DRAPER LAB, INC
ATTN: J BOYLE
ATTN: N TIBBETTS

CLEMSON UNIVERSITY
ATTN: P J MCNULTY

COMPUTER SCIENCES CORP
ATTN: A SCHIFF

DAVID SARNOFF RESEARCH CENTER, INC
ATTN: R SMELTZER

E-SYSTEMS, INC
ATTN: MAIN LIBRARY

EATON CORP
ATTN: R BRYANT

ELECTRONIC INDUSTRIES ASSOCIATION
ATTN: J KINN

GENERAL ELECTRIC CO
ATTN: B FLAHERTY
ATTN: L HAUGE

GENERAL ELECTRIC CO
ATTN: G GATI MD

GENERAL ELECTRIC CO
ATTN: DAREN NERAD

GENERAL ELECTRIC CO
ATTN: J MILLER

GENERAL RESEARCH CORP
ATTN: A HUNT

GEORGE WASHINGTON UNIVERSITY
ATTN: A FRIEDMAN

H M WEIL CONSULTANTS, INC
ATTN: H WEIL

HARRIS CORP
ATTN: J C LEE
ATTN: J W SWONGER

HARRIS CORPORATION
ATTN: E YOST
ATTN: W ABARE

HONEYWELL INC
ATTN: R JULKOWSKI

HONEYWELL SYSTEMS & RESEARCH CENTER
ATTN: R BELT

HONEYWELL, INC
ATTN: MS 725-5

HUGHES AIRCRAFT COMPANY
ATTN: E KUBO
ATTN: L DARDA

IBM CORP
ATTN: DEPT L75

IBM CORP
ATTN: J ZIEGLER

IBM CORP
ATTN: N HADDAD

IIT RESEARCH INSTITUTE
ATTN: I MINDEL

INSTITUTE FOR DEFENSE ANALYSES
ATTN: TECH INFO SERVICES

JAYCOR
ATTN: D WALTERS

JAYCOR
ATTN: R SULLIVAN

JAYCOR
ATTN: R POLL

JOHNS HOPKINS UNIVERSITY
ATTN: R MAURER

KAMAN SCIENCES CORP
ATTN. DASIAC
ATTN: E CONRAD

KAMAN SCIENCES CORPORATION
ATTN: DASIAC
ATTN: R RUTHERFORD

KEARFOTT GUIDANCE AND NAVIGATION CORP
ATTN: J D BRINKMAN

LEHIGH UNIVERSITY
2 CYS ATTN: DR D R YOUNG
2 CYS ATTN: DR R J JACCODINE

LITTON SYSTEMS INC
ATTN: F MOTTER

LOCKHEED MISSILES & SPACE CO, INC
ATTN: F JUNGA
ATTN: TECHNICAL INFORMATIION CENTER

LOCKHEED MISSILES & SPACE CO, INC
ATTN: E HESSEE
ATTN: G LUM ORG 81-63
ATTN: J CAYOT DEPT 81-63
ATTN: L ROSSI
ATTN: P BENE

LOCKHEED SANDERS, INC
ATTN: BRIAN G CARRIGG

LOGICON R & D ASSOCIATES
ATTN: D CARLSON

LORAL AERONUTRONIC
ATTN: TECHNICAL LIBRARY

LTV AEROSPACE & DEFENSE COMPANY
2 CYS ATTN: LIBRARY EM-08

MARTIN MARIETTA CORP
ATTN: J TANKE
ATTN: TIC/MP-30

MARTIN MARIETTA CORP
ATTN: S BUCHNER

MARTIN MARIETTA DENVER AEROSPACE
ATTN: P KASE
ATTN: RESEARCH LIBRARY

MARYLAND, UNIVERSITY OF
ATTN: H C LIN

MCDONNELL DOUGLAS CORP
ATTN: A P MUNIE DEPT 4100
ATTN: R L KLOSTER

MCDONNELL DOUGLAS CORPORATION
ATTN: P ALBRECHT

MESSENGER, GEORGE C
ATTN: G MESSENGER

MISSION RESEARCH CORP
ATTN: R PEASE

MISSION RESEARCH CORP
ATTN: J LUBELL
ATTN: W WARE

MITRE CORPORATION
ATTN: J R SPURRIER
ATTN: M FITZGERALD

NATIONAL SEMICONDUCTOR CORP
ATTN: F C JONES

NORDEN SYSTEMS, INC
ATTN: N RIEDERMAN
ATTN: TECHNICAL LIBRARY

NORTHROP CORPORATION
ATTN: J R SROUR

PACIFIC-SIERRA RESEARCH CORP
ATTN: H BRODE

PHYSITRON INC
ATTN: MARK CHRISTOPHER

PHYSITRON INC
ATTN: MARION ROSE

RAND CORP
ATTN: C CRAIN

RAND CORP
ATTN: B BENNETT

RAYTHEON CO
ATTN: D D LEE
ATTN: JOSEPH SURRO

RENSSELAER POLYTECHNIC INSTITUTE
ATTN: J HOWARD

RESEARCH TRIANGLE INSTITUTE
ATTN: M SIMONS

ROCKWELL INTERNATIONAL CORP
ATTN: V DE MARTINO
ATTN: YIN-BUTE YU

S-CUBED
ATTN: J M WILKENFELD

SCIENCE APPLICATIONS INTL CORP
ATTN: D MILLWARD
ATTN: DAVID LONG

SCIENCE APPLICATIONS INTL CORP
ATTN: J RETZLER

SCIENCE APPLICATIONS INTL CORP
ATTN: W CHADSEY

SCIENCE APPLICATIONS INTL CORP
ATTN: P ZIELIE

SCIENTIFIC RESEARCH ASSOC, INC
ATTN: H GRUBIN

SUNDSTRAND CORP
ATTN: C WHITE

SYSTRON-DONNER,
ATTN: SECURITY OFFICER

TECHNOLOGY DEVELOPMENT ASSOCIATES
ATTN: R V BENEDICT

TELEDYNE BROWN ENGINEERING
ATTN: G R EZELL
ATTN: LEWIS T SMITH

TEXAS INSTRUMENTS, INC
ATTN: J SALZMAN
ATTN: T CHEEK

TRW
ATTN: M J TAYLOR

TRW SPACE & DEFENSE SECTOR
ATTN: C BLASNEK
ATTN: DR D R GIBSON

TRW SPACE & DEFENSE SECTOR
ATTN: D M LAYTON
ATTN: HL DEPT LIBRARY

UNISYS CORPORATION-DEFENSE SYSTEMS
ATTN: P MARROFFINO

VISIDYNE, INC
ATTN: C H HUMPHREY
ATTN: W P REIDY

FOREIGN

FOA 2
ATTN: B SJOHOLM